Cell Communication and Signaling

RESEARCH Open Access

Synergic action of MicroRNAs and Wnts delivered by motor neuron EVs in promoting AChR clustering

Rachele Agostini[1†], Paola Ceccaroli[1†], Emanuela Polidori[1†], Manuela Ferracin[2,3], Ilaria Pace[2], Serena Maggio[1], Andrea Cioccoloni[1], Michela Battistelli[1], Giulia Matacchione[4], Matilde Sbriscia[4], Fabiola Olivieri[4,5], Fabrizia Cesca[6,7], Vilberto Stocchi[8] and Michele Guescini[1*]

Abstract

Background The neuromuscular junction (NMJ) establishment occurs through complex communication events between motor neurons and muscle fibers; however, the molecular mechanisms leading to NMJ formation have yet to be fully elucidated. Little is known about the significance of extracellular vesicles (EVs) in mediating the interaction between motor neurons and muscle fiber in the NMJ establishment; this study investigates the role of motor neuron-derived EVs during the earliest stages of NMJ formation.

Methods NSC-34 cells have been used as a model of motor neurons; EVs have been isolated during neurite development using a serial ultracentrifugation protocol specifically adjusted to isolate large and small EVs. Isolated EVs were quantified through Nanoparticles Tracking Assay and characterized by Western Blot and TEM analyses. The microRNA (miRNA) cargo of EV subpopulations was identified by small-RNA sequencing and the predicted miRNA downstream targets were investigated.

Results NGS analysis of small RNAs carried by NSC-34-derived EVs identified a total of 245 EV specific miRNAs, most of which are up-regulated in NSC-34 cells and EVs during neurite stretching. Target prediction analysis evidenced how these miRNAs synergically target the Wnt signaling pathway. Moreover, we found that NSC-34-derived EVs carry Wnt proteins, including Wnt11, Wnt4 and Wnt3a. Since several studies suggested a role for the Wnt-associated signaling network in NMJ formation, we investigated the potential role of NSC-34 EVs in NMJ development and demonstrated that EV administration to myotubes increases acetylcholine receptor (AChR) cluster formation, as revealed by immunofluorescence staining with α-bungarotoxin. Moreover, myotube treatment with NSC-34-derived EVs led to GSK3β and JNK phosphorylation, followed by β-catenin nuclear translocation, suggesting that neuron-derived EVs can induce AChR clustering through Wnt pathway activation.

[†]Rachele Agostini, Paola Ceccaroli and Emanuela Polidori contributed equally to this work.

*Correspondence:
Michele Guescini
michele.guescini@uniurb.it

Full list of author information is available at the end of the article

Conclusion These data demonstrate that EVs released from differentiated motor neurons carry multimodal signals, miRNAs, and Wnts, which can stimulate AChR clustering in myotubes, a fundamental preparatory stage for NMJ formation. These new data highlight that EVs may play a role in the NMJ establishment and function under physiological and pathological conditions, particularly neurodegenerative diseases.

Keywords Neuromuscular junctions, Wnt signalling, Agrin, β-catenin, Acetylcholine receptor, Extracellular vesicles

Background

The neuromuscular junction (NMJ) is a chemical synapse formed between motor neuron and skeletal muscle. This interface allows the conversion of electrical impulses into chemical messages through neurotransmitter acetylcholine (ACh), which in turn enables the conversion of neuronal electrical signals into muscle-derived mechanical responses via downstream calcium-induced calcium release [1, 2]. Proper NMJ formation and maintenance are essential for physical mobility and daily life.

NMJ formation is an elaborate process in which anterograde (presynaptic) and retrograde (postsynaptic) signals shepherd neuron-muscle interplay through distinct developmental steps. During embryonic development, motor neurons penetrate peripheral regions to reach myotubes and then innervate muscles at the end-plate band, a region where axon terminals branch into synaptic varicosities apposed to foldings of the muscle junctional folds. Before NMJ takes place, both motor terminals and muscle membrane undergo morphological changes: *i*) Presynaptic zones begin to accumulate synaptic vesicles containing acetylcholine; *ii*) Postsynaptic zones undergo acetylcholine receptor (AChR) enrichment; at first, these receptors are diffused on all the muscle membrane, and then AChRs are clustered into distinct oval-like plaques. On the whole, this process is called pre-patterning [1–3]. A correct NMJ growth is the result of both pre- and post-synaptic differentiation processes, as plaque formation can be induced neuronally at contact sites or occur "spontaneously" as aneural AChR "hotspots" on the muscle fibre [4]. Recent studies have shown that a complex network of molecular signals participates in regulationing events that lead to the formation of NMJs. For example, the motor neuron-derived Agrin binds to muscle low-density lipoprotein receptor-related protein 4 (Lrp4) leading to the activation of MuSK and AChR clustering in the postsynaptic membrane [5, 6]. Moreover, growing evidence suggests that some Wnt proteins cooperate with Agrin in NMJ development [7]. Wnts are glycoproteins known to activate a canonical signalling pathway that is β-catenin (Ctnnb1) dependent, as well as several non-canonical pathways [8]. At the vertebrate NMJ, Wnts activate the receptor complexes formed by the muscle-specific tyrosine kinase MuSK and Lrp4, or MuSK and classical Frizzled (Fzd) receptors [7, 9–11]. Furthermore, it has recently been demonstrated that Wnt4, -9a, and −11 directly interact with MuSK, and this interaction enhances AChR clustering in muscle cells [12], these data are in line with previous evidence demonstrating that ectopic MuSK expression is sufficient to induce AChR clusters in the absence of the nerve when bound with Agrin [13]. Altogether, these results suggested that MuSK might be activated by ligands other than Agrin to regulate pre-patterning.

Despite intensive research activities, the molecular mechanisms leading to NMJ formation have not been fully elucidated yet: a new set of experiments suggested that, due to post-translational lipid modifications, Wnts can be loaded in membranous vesicles for secretion and extracellular travelling [14–17]. Indeed, recent evidence demonstrated that Wnt1, can be trafficked in exosomes through binding to the transmembrane exosomal protein, Evi, and in turn, Wnt1 can be transferred from pre- to post-synaptic cells *via* vesicle secretion in *Drosophila* larval NMJs [15, 18, 19]. A similar exosome-mediated mechanism for the transfer of transmembrane protein across cells was suggested for synaptotagmin-4 (Syt4), which functions in postsynaptic muscles to mediate activity-dependent presynaptic growth and potentiation of quantal release. A retrograde signal mediated by Syt4 was transmitted from presynaptic boutons to postsynaptic muscle compartments at *Drosophila* larval NMJ through anterograde delivery of Syt4 via exosomes, indicating that these exosomes were delivered to the post-synaptic membrane [20]. A similar process has been previously observed in the immune system [21].

Exosomes are a sub-population of extracellular vesicles (EVs) generated by the inward budding of endosomal limiting membranes into multivesicular bodies (MVBs). MVBs can either fuse with lysosomes to degrade obsolete cellular material or with the plasma membrane to release vesicle-associated signalling components [22, 23]. Exosomes and in general EVs have gained attention owing to their potential role in cell-to-cell communication by transferring proteins, lipids, DNA, mRNAs and microRNAs (miRNAs) to target cells, and each of them may be involved in modulating target-cell phenotype.

In line with these new findings, miRNAs have not only emerged as intracellular regulators of gene expression, but protein and miRNA-containing vesicles have been suggested as a new molecular mechanism for communication between cells in the nervous system [24, 25]. MiRNAs regulate various key cellular signalling networks such as Wnt, transforming growth factor-β and

Notch and control stem cell activity in maintaining tissue homeostasis [26]. The discovery that miRNAs are critical to motor neuron function and survival [27] led to the study of miRNA participation in NMJ formation and stabilisation. Consistent with this theory, Nesler et al. [28] showed that five miRNAs act in an activity-dependent manner at the NMJ within *Drosophila* larvae, including miR-8. Notably, the Authors showed that miR-8 directly targets and suppresses Wingless (Wg) expression, an essential gene for NMJ development and plasticity. MiR-8, along with miR-289 and miR-958, silenced Leukocyte-antigen-related-like (Lar) expression, important for synaptic growth and motor axonal extension [18, 19, 28, 29].

In this study, we investigated the crosstalk between myotubes and motor neurons during NMJ development, focusing on identifying the miRNAs loaded into large and small EVs (lEVs and sEVs) secreted from developing motor neurons. We identified several miRNAs implicated in motor neuron and NMJ development, and we shed light on the molecular mechanism underlying the crosstalk between Wnt-signalling (both canonical and non-canonical) and miRNAs. Overall, our data suggest that motor neuron-derived EVs carry multimodal signals, including miRNAs and Wnts, which are fundamental in the preparatory stage of NMJ establishment.

Methods

Cell cultures

The C2C12 adherent mouse myoblast cell line was grown in High Glucose Dulbecco's modified Eagle's medium (DMEM; Lonza™ BioWhittaker™) supplemented with 1% penicillin/streptomycin (P/S, Euroclone), 2 mM glutamine and 10% heat-inactivated fetal bovine serum (FBS; Euroclone) in 5% CO_2 atmosphere at 37 °C. When cells were 90% confluent, C2C12 differentiation was triggered by replacing 10% FBS with 2% horse serum (HS; Euroclone) as previously described [30], and cells were cultured for up to 7 more days.

The NSC-34 adherent mouse motor neuron cell line was maintained in DMEM (Sigma-Aldrich) supplemented with 10% FBS and 1% P/S and cultured at 37 °C under 5% CO_2. For NSC-34 differentiation, cells were seeded onto collagen (Sigma-Aldrich) coated plates and when they reached 60% confluence, the growth medium was replaced with Neurobasal (ThermoFisher Scientific) differentiating medium supplemented with 1% P/S and 0.5 mM L-glutamine (ThermoFisher Scientific) and cultured for up to 7 more days. For both C2C12 and NSC-34 cell cultures the differentiation media were changed every two days.

Co-culture experiments were performed by using Transwell permeable supports with a membrane filter of 0.4 μm pores interposed between the two cell lines: C2C12 myotubes at bottom and differentiated NSC-34 cells above. After 48 h co-culture, myotubes were harvested and RNA extracted for gene expression analysis.

Stable transfection of HEK293 cells with Wnt11

Hek293 cell stable transformation was achieved by using the plasmid encoding Wnt11 in fusion with an HA tag (Sino Biologicals, cat. no. HG12056-CY) and the TransIT-X2 kit (Mirus), following the manufacturer's instructions. The Hek293 cells were grown in DMEM supplemented with 10% FBS at 37 °C with 5% CO_2 for 48 h, after which 100 ng/mL hygromycin B was added to select for stable transformants.

Spinal cord explant

Spinal cord explants were isolated from E13.5 C57BL/6J embryos by longitudinal cuts along the spinal cord, the ventral horn was separated from the dorsal horn and placed in well as transverse sections of up to 1 mm thickness. Before plating the spinal cord, the wells were coated using 1.5 ng/ml polyornithine (Sigma-Aldrich) in PBS overnight, replaced with laminin (Sigma-Aldrich), 1:333 in water overnight, and then filled with explant medium (Neurobasal, ThermoFisher Scientific) supplemented with 1% P/S, 1% Glutamax, 2% B27, 25 ng/ml brain-derived neurotrophic factor (BDNF) until the day on which culture was started. Cultures were maintained at 37 °C and 5% CO_2, and the growth medium was refreshed every 2 days. Experiments were carried out in accordance with the guidelines established by the European Communities Council (Directive 2010/63/EU of 22 September 2010).

Immunofluorescence microscopy

For immunofluorescence microscopy, the cells were grown on glass coverslips, fixed in 4% paraformaldehyde/PBS permeabilized in PBS + 0,1% Triton X-10, and incubated in blocking solution 4% Bovine Serum Albumin (BSA, Sigma-Aldrich) for 1 h. Then, samples were stained with the primary antibody for 1 h at 4 °C, followed by separate incubation with secondary antibody for 1 h at room temperature. Stained samples were mounted in Mowiol 4–88 (Sigma-Aldrich) and photographed using a DC300F digital camera connected to a Fluorescence microscope (IM50 software Leica, Wetzlar, Germany).

Nuclear DNA was stained with 4,6-diamino-2-phenylindole (DAPI, 1:1000 dilution, Sigma-Aldrich) or Hoechst 33342 (1:400 dilution, Sigma-Aldrich). To assess acetylcholine receptor (AChR) clusterization, C2C12 were stained for 1 h with α-Bungarotoxin Alexa Fluor™ 488 conjugate (3μg/mL dilution, cod. B13422 ThermoFischer Scientific) and displayed using a confocal laser microscope (SP8, Leica Microsystems GmbH, Wetzlar, Germany). Subsequently, the number, areas and intensity

of the AChR clusters were measured using Image J software. Finally C2C12 myotubes treated with NSC34-derived sEVs, were stained with Active β-catenin (1:50, Anti-Active-β-Catenin Antibody, clone 8E7 Millipore) to assess nuclear-boud/active β-catenin.

Extracellular vesicle isolation

EV isolation was carried out following the Minimal Information for Studies of Extracellular Vesicles guidelines developed by the International Society for Extracellular Vesicles (ISEV) in 2023 [31]. Specifically, the cell-conditioned medium was collected and purified by two serial centrifugations for 15 min at 1,000 × g and 15 min at 2,000 × g to remove debris and apoptotic bodies.

Then, to pellet large EVs (lEVs), the supernatant was centrifuged at 12,000 × g for 30 min and 18,000 × g for 30 min. The pellets resulting from both centrifugations were joined together, resuspended in phosphate-buffered saline (PBS) and further ultracentrifuged at 15,000 × g for 30 min to wash the sample.

To isolate small EVs (sEVs) the collected supernatant was subjected to ultracentrifugation at 100,000 × g for 2 h. The crude sEVs pellet was resuspended in a large volume of PBS and furtherly ultracentrifuged at 100,000 × g for 2 h to wash the sample. During the whole protocol, temperature was maintained at 4 °C.

Nanoparticle tracking assay (NTA)

NTA measurements were performed with a NanoSight LM10 (NanoSight, Amesbury, United Kingdom) and three videos of either 30–60 s were recorded of each sample. All measurements were performed at RT, never above 25 °C. The NTA 3.1 software (NanoSight) was used for capturing and analysing the data, which are presented as the mean ± SD of the three video recordings. Samples containing high particle numbers were diluted before analysis and the relative concentration was then calculated according to the dilution factor. Beads of 100 nm and 400 nm diameters (Malvern Instruments Ltd., Malvern, UK) were used as control.

Transmission electron microscopy

For a detailed morphological analysis, vesicles were processed for transmission electron microscopy observation using the conventional negative staining procedure. EVs were immediately fixed with 2.5% glutaraldehyde for 30 min and later adsorbed to formvar carbon-coated 200 mesh grids (Agar Scientific Ltd., Stansted, UK) for 10 min. Subsequently the grids were incubated with 2% (w/v) sodium phosphotungstate for 1 min and the liquid excess was removed with filter paper. After negative staining, specimens were observed by means of a Philips CM10 transmission electron microscope at 80 kV.

Small RNA seq analysis

SmallRNA libraries were prepared from 12NSC-34 EV samples using TruSeq Small RNA Library PrepKit v2 (Illumina, RS-200-0012/24/36/48), according to manufacturer's indications. Briefly, 20 ng of purified RNA were linked to RNA 3' and 5' adapters, converted to cDNA and amplified using Illumina primers containing unique indexes for each sample. Each library was quantified using Agilent Bioanalyzer and High Sensitivity DNA kit (Agilent, 5067 – 4626) and an equal number of libraries were pooled together. Size-selection was performed to keep fragments between 130 and 160 bp. The library pool was quantified with Agilent High Sensitivity DNA kit, diluted to 1.8 pM and sequenced using NextSeq® 500/550 High Output Kit v2 (75 cycles) (Illumina, FC-404-2005) on Illumina NextSeq 500 platform. Raw data generated from the Illumina NextSeq 500 system were converted to FASTQ format. After a quality check, which was performed with FastQC tool (https://www.bioinformatics.babraham.ac.uk/), the adapter sequences were trimmed using Cutadapt (http://cutadapt.readthedocs.io/). In this step, sequences shorter than 10 nucleotides were also removed. Read mapping was performed using the STAR algorithm [32]. The reference genome was constituted by mouse microRNAs sequences from the miRbase 21 database (http://www.mirbase.org/). Raw counts from mapped reads were obtained using the htseq-count script from the HTSeq tools (http://www-huber.embl.de/HTSeq/); raw counts were further normalised using DESeq2 bioconductor package (http://bioconductor.org/) and analysed using Genespring GX software v. 14.8 (Agilent Technologies) for PCA generation, class comparison and heatmap analysis. The log2 normalized miRNA expression data are available in Additional file 1. A fold-change > 1.5 and $p < 0.05$ at moderated T-Test were applied to identify miRNAs significantly differentially expressed. The list of predicted miRNA targets was identified using the prediction algorithm DNA Intelligent Analysis (DIANA) DIANA-microT-CDS (v5.0). The predicted miRNA targets were annotated into functional pathways using DIANA-miRPath (v2.0) (http://diana.imis.athenainnovation.gr/DianaTools/index.php?r=site/index).

RNA isolation and quantification

For miRNA quantification analyses, EVs were first treated with RNase A (Qiagen) and then total RNA was extracted from the EVs by using the RNAZOL DIRECT CLEAN UP kit (FMB, Fisher Molecular Biology) and reverse transcribed with the miRCURY LNA Universal RT microRNA PCR kit (Exiqon). The optional UniSP6 RNA spike-in oligonucleotide was added to each reaction and used for normalisation. Quantitative RT-PCRs were performed with the miRCURY LNA SYBR® Green PCR

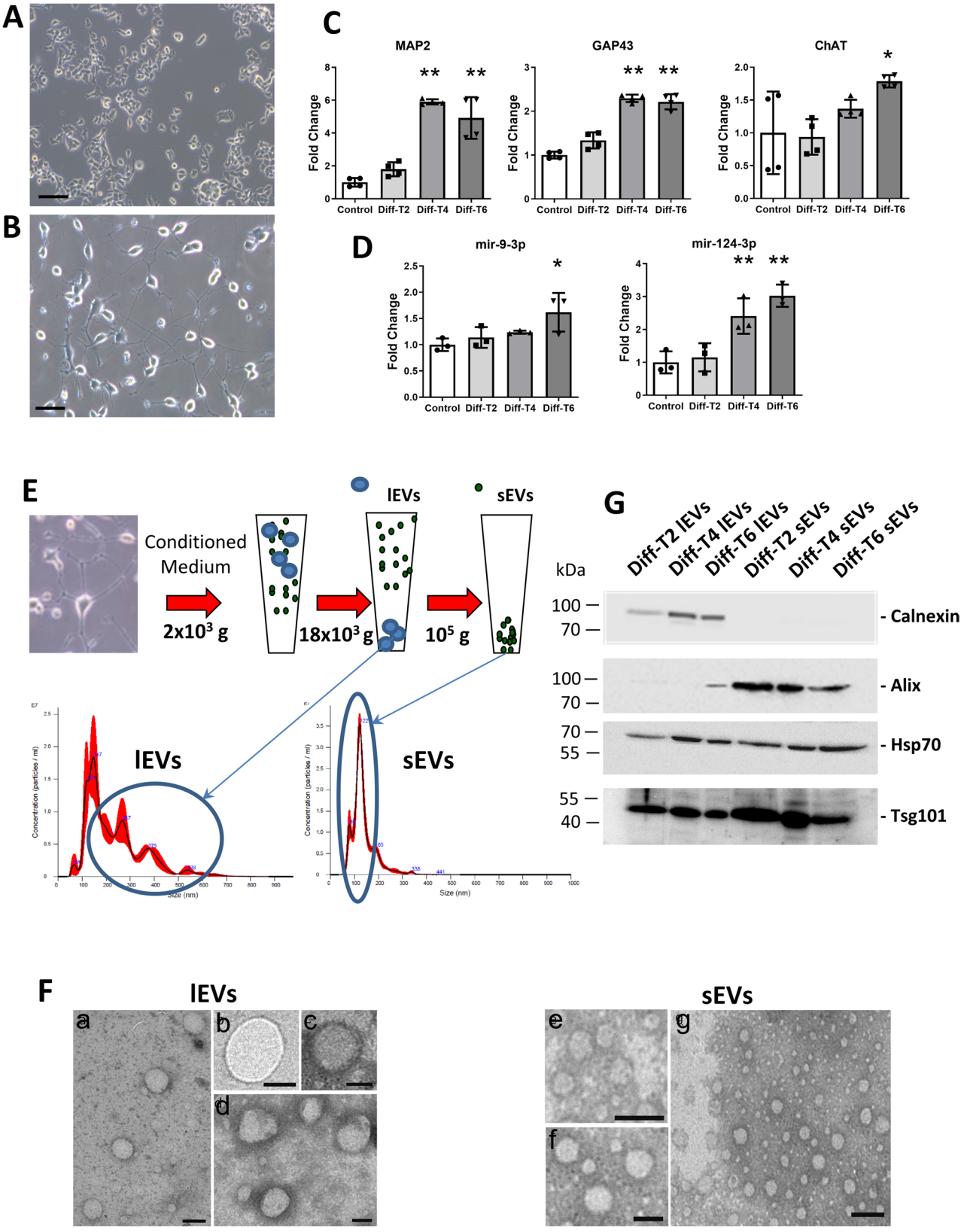

Fig. 1 (See legend on next page.)

(See figure on previous page.)

Fig. 1 Quantification and characterization of the EVs released during NSC-34 differentiation. Light microscopy images of the NSC-34 cells before (**A**; size bar: 200 µm) and after (**B**; size bar: 100 µm) inducing neuron process outgrowth. In particular, picture B clearly shows neurite development and branching obtained after 4 days of differentiation. Cell viability assayed after 4 days of differentiation is shown in Additional file 10. **C**) Time course of gene expression analysis of the key differentiation markers *MAP2* (microtubule-associated protein), *GAP-43* (growth associated protein 43) and *ChAT* (choline acetyltransferase), and (**D**) MotomiRs miR-9-3p and miR-124-3p in differentiating NSC-34 cells ($n = 3$, * $p < 0.05$, ** $p < 0,01$; one-way ANOVA test followed by Dunnett's post-hoc test). The process of differentiation was carried out on NSC-34 cells for two days (Diff-T2), and four days (Diff-T4), and at each of these time points, the collection and characterisation of EVs was undertaken. **E**) Schematic representation of the serial ultracentrifugation protocol used to harvest EVs from conditioned medium, and separate large from small EVs (lEVs and sEVs, respectively); the NTA distribution plots of vesicle hydrodynamic diameter revealed the difference in size between lEVs and sEVs. **F**) The size distribution of lEVs and sEVs was also confirmed using transmission electron microscopy (in the panels b, c, d, e and f the size bar corresponds to 100 nm, while in the panels a and g the bar corresponds to 200 nm). **G**) Western blots analyses show the presence of the well-established EV markers: Alix, Hsp70 and Tsg101, and the negative marker for sEVs, Calnexin (5 µg of total proteins were loaded per lane). Molecular weight markers (kDa) are indicated. Original, uncropped immunoblots are reported in Additional file 7- Fig. S1

Kit and miRCURY LNA miRNA PCR Assays (Qiagen) specific for each miRNAs analysed. The qRT-PCR conditions were the following: initial incubation step at 95 °C for 10 min followed by 50 cycles consisting of two steps at 95 °C for 10 s and 60 °C for 60 s. Cq were determined using the Cy0 method, performed according to the ΔCq method [33].

Total RNA from cell bodies was isolated by using E.Z.N.A. Total RNA kit (VWR Omega). cDNA was obtained using the Maxima Reverse Transcriptase kit (ThermoFisher Scientific). qRT-PCR amplifications were conducted using Sensi-FAST SYBR Green (Bioline); the final concentration of the primers used for the gene target quantification (Additional file 2) was 400 nM.

The amplification protocol consisted of the following steps: initial incubation at 95 °C for 2 min, followed by 40 cycles (95 °C for 5 s; 60 °C for 5 s; 72 °C for 10 s). All the amplification reactions were performed using a LightCycler 480 (Roche).

Melt-curve analysis was used to confirm the specificity of amplification and lack of primer dimers. Relative quantification of mRNA expression levels was conducted according to the ΔCq method. The expression level of GAPDH was used as a reference gene for the normalisation of the mRNA target analysed [34]. In all RNA extractions, a DNase I digestion (Ambion) was performed to eliminate DNA contamination.

Western blotting analysis

Whole proteins were isolated from the organic phase of EVs or cell bodies from QIAzol Reagent-lysed samples (Qiagen User Protocol RY16 May-04) after phenol separation of RNAs contained in aqueous phase and DNA in the interphase. The protein pellet was resuspended in ISOT buffer (8 M urea, 4% CHAPS, 65 mM DTE (1,4-Dithioerythritol), 40 mM Tris base supplemented with SigmaFAST Protease Inhibitor Cocktail (Sigma-Aldrich) and 10 mM Sodium Fluoride). The obtained suspension was sonicated one time with 10 s pulse and then centrifuged at 12,000 × g for 10 min (4 °C).

The cell body protein concentration was determined by the Bradford assay using Bio-Rad Protein Assay Dye Reagent Concentrate (BioRad). To assess lEV and sEV protein concentration an aliquot of 20 µl of each sample was mixed with 20 µl of the BCA Working Reagent (ThermoFisher Scientific) and the tubes were then incubated at 60 °C for 1 h. After the transfer to a 96-well plate, the absorbance was measured at 565 nm on a microplate reader (BioRad). Equal protein quantities were separated on 12% SDS-PAGE gel and transferred to Immuno blot Polyvinylidene Difluoride membranes, 0.2 µm (PVDF, ThermoFisher Scientific). Primary antibodies used are listed in Additional file 3. Membranes were incubated with the primary antibodies overnight at 4 °C followed by washing and application of the appropriate HRP-conjugated secondary antibodies. Immune complexes were visualised using Clarity Western ECL Substrate (BioRad) and the ChemiDoc MP Imaging System (BioRad).

Statistics

Statistical analysis was performed using GraphPad Prism 8. Normality of data distribution was assessed with the Shapiro-Wilk test. Differences between group mean were assessed with a 2-tailed Student's t-test for unpaired observation. More than 2 groups were compared using one-way ANOVA for repeated measures with Dunnett's or Bonferroni post hoc analysis. Results are presented as mean ± standard deviation (SD). The level of significance was set at $p \leq 0.05$.

Results

NSC-34 cells release large and small EVs during neurite development and branching

The NSC-34 cells express many of the morphological and physiological properties of motor neurons, including extension of processes, formation of contacts with cultured myotubes, synthesis and storage of acetylcholine, support of action potentials, induction of myotube twitching, and expression of neurofilament proteins [35].

In our hands, undifferentiated NSC-34 cells did not reveal spontaneous neurite growth (Fig. 1A), whereas following differentiation, induced by shifting cells from proliferation to neurobasal medium, NSC-34 cells started to develop neurites that progressively stretched and

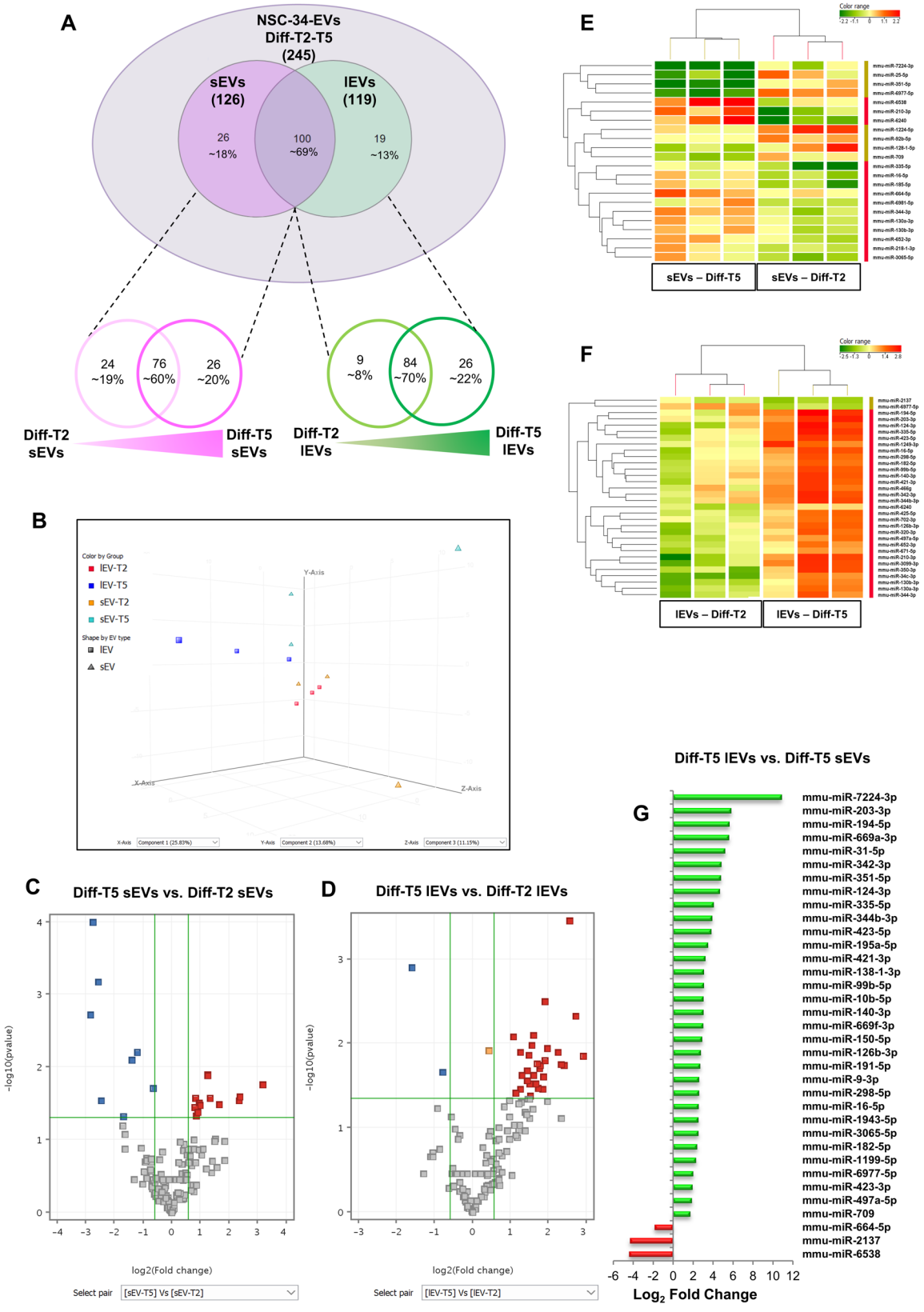

Fig. 2 (See legend on next page.)

(See figure on previous page.)

Fig. 2 NGS analysis of miRNAs loaded into EVs and released during the NSC-34 differentiation process. **A**) Descriptive analyses of miRNAs detected in small and large EV samples ($N = 12$) at two differentiation time points (Diff-T2 and -T5) using small RNA seq. In the Venn diagrams, each area reports the number (%) of miRNAs detected in the corresponding group in at least two samples ($N = 3$ per group). The upper part of the panel A shows the comparison of the miRNAs detected in lEVs and sEVs regardless the differentiation time, while in the lower part lEVs and sEVs have been analysed separately, and the differences between the number of miRNAs detected at Diff-T2 and Diff-T5 have been reported. **B**) Unsupervised PCA analysis revealing the similarity between groups. The progressive separation of EV samples collected at Diff-T5 can be appreciated. **C**) and **D**) Volcano plot evidencing the number of miRNAs differentially abundant (Moderated t-test < 0.05, fold change > 1.5) in small and large EVs, respectively, when comparing Diff-T5 vs. Diff-T2. **E**) and **F**) Heatmap representation of the differentially abundant miRNAs in three EV replicate samples during neuronal differentiation. Red color indicates greater abundance, green color indicates lower abundance. The Panel G reports the list of miRNAs differentially abundant in large and small EVs at Diff-T5 differentiation and their relative expression. The X-axis represents the Log2 fold change in miRNA counts between Diff-T5-lEVs vs. Diff-T5-sEVs. Green bars are miRNAs more abundant in large EVs at Diff-T5, red bars are miRNAs more abundant in sEVs at Diff-T5

branched (Fig. 1B). Along with the NSC-34 morphological differentiation, we observed the up-regulation of cytoskeletal marker genes, as evidenced by the increased mRNA levels of *MAP2* (microtubule-associated protein), *GAP-43* (growth-associated protein 43) and the motor neuron differentiation marker *ChAT* (choline acetyltransferase) at 4–6 days after the switch to neurobasal medium (Fig. 1C). Moreover, neuron-specific miR-9-3p and miR-124-3p were up-regulated during motor neuron development (Fig. 1D), in accordance with previous studies showing that these two miRNAs are abundantly expressed in the mammalian nervous system and are mainly involved in controlling neuron fate and synaptic morphology [36, 37].

Based on the above results, NSC-34 cells were used as a model to study the release of EVs during motor neuron development. To this end, conditioned medium was harvested at various time points of NSC-34 differentiation and EVs were purified using a serial ultracentrifugation protocol precisely adjusted to remove cellular debris and isolate large and small EVs (lEVs and sEVs; Fig. 1E). The nanoparticle tracking assay of purified EVs showed that sEVs had a hydrodynamic diameter of about 122 nm. In comparison, lEVs showed a much more variable size with an average diameter of 170 nm (Fig. 1E). Furthermore, when examined by transmission electron microscopy (TEM) using negative staining, the isolated EVs appeared as closed rounding vesicles delimited by membrane structures; sEVs appeared as vesicles with an outer dense wall and an inner less dense region of approximately 90–120 nm in diameter, whereas lEVs presented a larger and variable size than sEVs of about 140–200 nm in diameter and some of them displayed an electron-dense material delimited by well-defined membrane structure (Fig. 1F). These data are in agreement with common EV features reported in literature [38]. Finally, western blot analysis showed that sEVs are negative for calnexin, a marker of the endoplasmic reticulum and positive for Alix; moreover, sEVs and lEVs are both positive for Hsp70 and Tsg101, two well-defined EV markers (Fig. 1G).

Analysis of EV-miRNAs released during NSC-34 differentiation

Since EVs can mediate intercellular communication through their cargo of miRNAs, we performed a small-RNA sequencing experiment to examine the whole miRNA cargo of EVs released during NSC-34 motor neuron development. We analysed three replicates of four EV samples ($n = 12$), including lEVs and sEVs released at early (Diff-T2) and late (Diff-T5) NSC-34 differentiation time (Additional file 1). A total of 245 miRNAs were detectable in at least two samples. Firstly, the miRNA segregation into the two EV populations, without accounting for the differentiation time, was analysed: of the 245 miRNAs detected, 26 miRNAs (17.9%) were retained only in sEVs, 19 miRNAs (13.1%) were packaged only in lEVs, and 100 miRNAs (69%) were present in both vesicle populations (Fig. 2A, Additional file 4). These data suggest that a fraction of miRNA is specific for either sEVs or lEVs.

Regarding the motor neuron development process, the analysis of the miRNAs released in small and large EVs showed that 60.3% (76 miRNAs) are commonly released at both Diff-T2 and Diff-T5 differentiation times, whereas the remaining miRNAs are differentially abundant in early and late NSC-34 differentiation EVs (Fig. 2A, Additional file 5 and 6).

The unsupervised Principal Component Analysis (PCA) conducted on all samples demonstrated a progressive distance between samples at Diff-T5 and confirmed the differences between the cargo of small and large vesicles (Fig. 2B). We then focused on the identification of the miRNAs differentially abundant in small and large EVs as a function of the differentiation time. We compared Diff-T5 sEVs vs. Diff-T2 sEVs and Diff-T5 lEVs vs. Diff-T2 lEVs. Of the total 126 miRNAs found in the sEVs, 14 miRNAs were significantly more abundant in Diff-T5 and 8 miRNAs in Diff-T2, as evidenced by volcano plot and heatmap analysis (Fig. 2C and E). Instead, of the total 119 miRNAs found in lEVs 30 out of 32 differentially abundant miRNAs were upregulated at the late time of differentiation (Fig. 2D and F). This evidence suggests that the number of secreted miRNAs increases during NSC-34 differentiation, with the most noticeable increase occurring in lEVs compared to sEVs (Fig. 2). This

observation was confirmed when we compared the miRNAs significantly modulated in Diff-T5 lEVs vs. Diff-T5 sEVs (Fig. 2G), confirming that miRNA secretion during neuronal differentiation is both stage and EV-type specific.

Functional analysis and gene expression validation of the differentially modulated EV-miRNAs

It has been suggested that miRNAs packaged into EVs can modulate the phenotype of recipient cells. To obtain a picture of the pathways possibly regulated by EV-miRNAs released during NSC-34 differentiation [39], two different web-based analytic tools were used, specifically DIANA miRPath [40] and miRSystem [41]. Moreover, since NSC-34 cells express motor neuron-like features mainly at late differentiation step, only the miRNAs significantly up-regulated in Diff-T5-sEVs and -lEVs were used as a query for the in silico search.

Based on these algorithms, we were able to identify the putative targets of the EV-miRNAs and their enriched pathways. Among the significantly enriched pathways, there are pathways known to have a key role in motor neuron development and intercellular communication, such as axon guidance, neurotrophin, Wnt and TGF-β (Fig. 3A) [42]. To further support these findings, the expression of miRNAs regulating these pathways (miR-9-3p, -16-5p, -335-5p, -669a-3p, -344-3p, -218-1-3p, -124-3p, -709, -34c-3p, -185-5p) were validated by

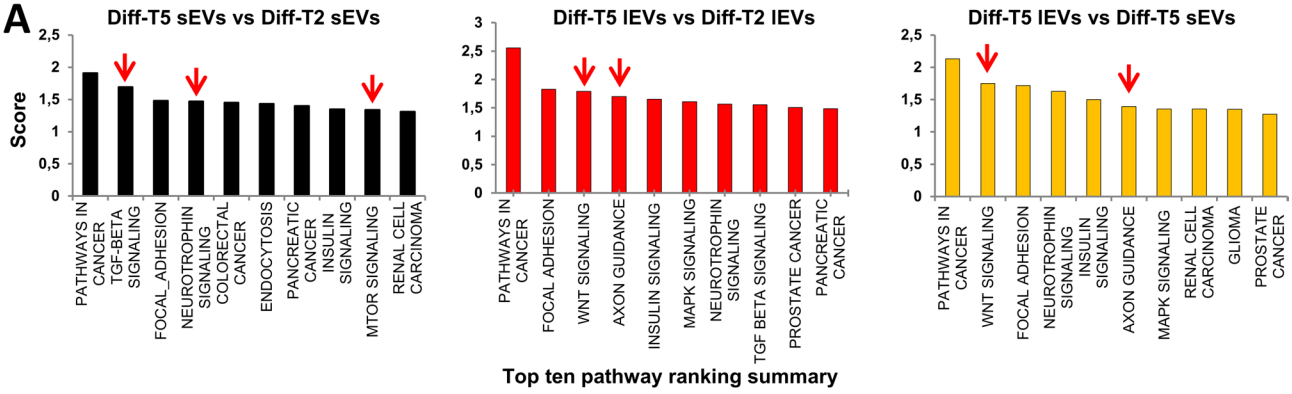

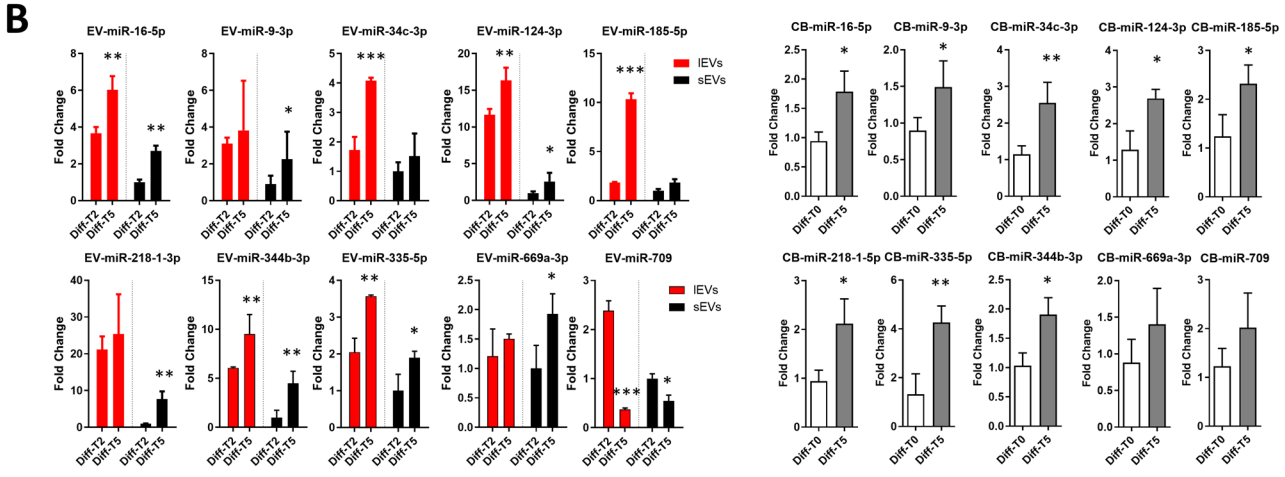

Fig. 3 Dissecting the complex signals carried by neuron-derived EVs during NSC-34 differentiation. **A**) miRNAs significantly modulated in lEVs and sEVs collected from late stage of the NSC-34 neuron process outgrowth compared to early stage development using DIANA-mirPath v.3 (https://dianalab.e-ce.uth.gr/html/mirpathv3/). DIANA-mirPath is a miRNA pathway analysis web-server, providing accurate statistics, to predicted miRNA targets (in CDS or 3'-UTR regions) provided by the DIANA-microT-CDS algorithm or even experimentally validated miRNA interactions derived from DIANA-TarBase. In the three panels top ten pathway rankings were reported. **B**) Since, the prediction analysis of the significantly modulated EV-miRNAs, obtained by NGS, suggested that Axon guidance, neurotrophin, Wnt and TGF-β signalling pathways could be the targets of the miRNAs loaded into NSC-34-derived EVs, qRT-PCR analyses of selected key miRNAs (miR-9-3p, -16-5p, -335-5p, -669a-3p, -344b-3p, -218-1-3p, -124-3p, -709, -34c-3p, -185-5p) were performed both in cell bodies and EVs with the aim to confirm miRNA expression. MiRNA expression analysis performed in lEVs and sEVs at early (Diff-T2) and late (Diff-T5) is reported on the left part of the panel B ($n = 3$, * $p < 0.05$, ** $p < 0,01$; Diff-T5 vs Diff-T2 were compared by t-test for lEVs and sEVs separately); in the right part of the panel B, miRNA expression levels were quantified in cell bodies ($n = 3$, * $p < 0.05$, ** $p < 0.01$; t-test)

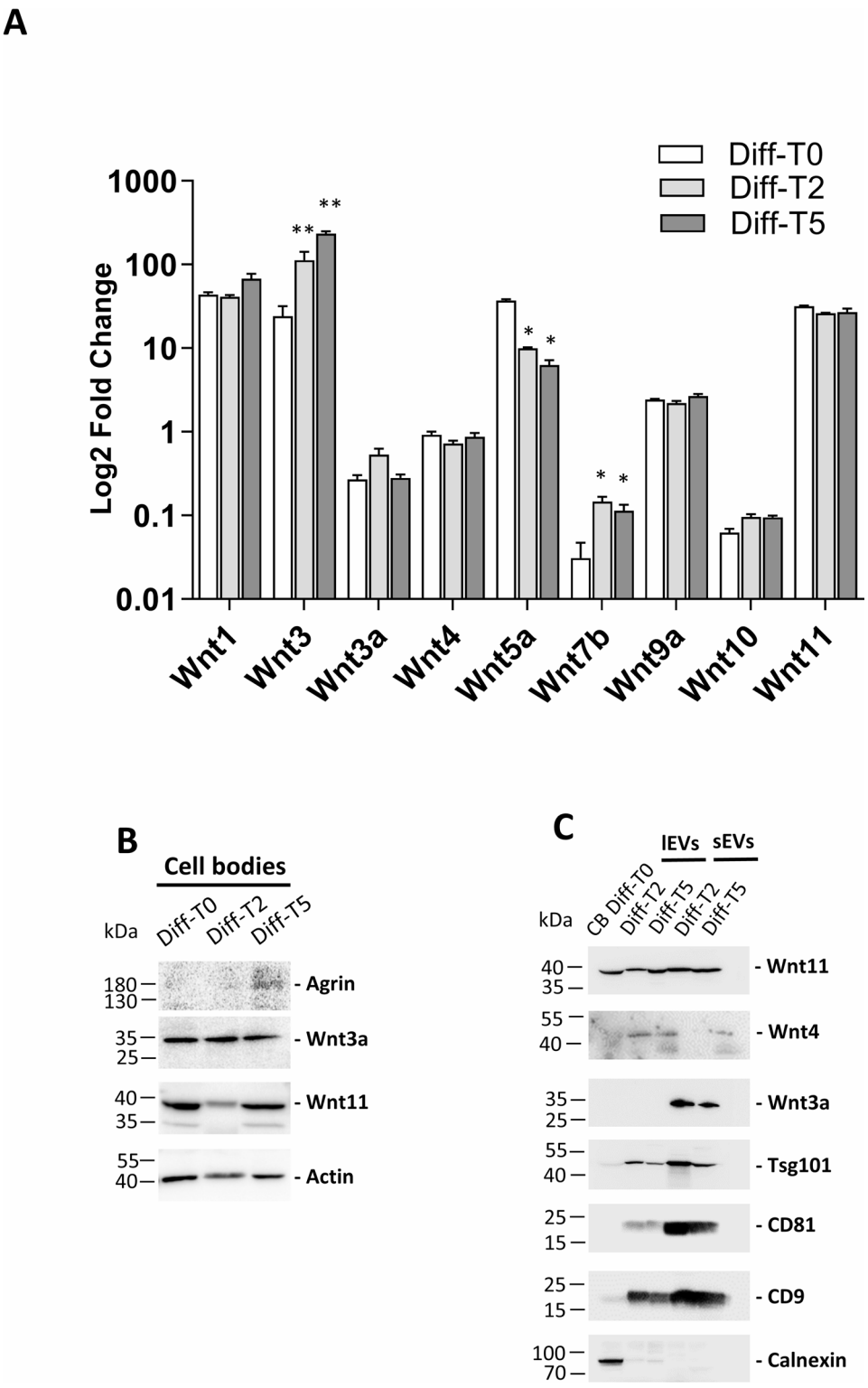

Fig. 4 (See legend on next page.)

qRT-PCR both in cell bodies and EVs released during NSC-34 differentiation. Quantitative RT-PCR confirmed the NGS results, and most of the analysed miRNAs were up-regulated in NSC-34 cell bodies and EVs along with neurite stretching (Fig. 3B). These data confirm that a number of miRNAs regulated during NSC-34 differentiation and involved in motor neuron maturation are also loaded into EVs suggesting that they could have a role in

(See figure on previous page.)

Fig. 4 Expression analysis of Wnts during NSC-34 differentiation. (**A**) Gene expression analysis of Wnt isoforms in NSC-34 whole cell during neuron process outgrowth (Diff-T0: undifferentiated NSC-34 cells; Diff-T2: NSC-34 switched to neurobasal medium for 2 days; Diff-T5: NSC-34 switched to neurobasal medium for 5 days; $n = 3$, * $p < 0.05$, ** $p < 0{,}01$; one-way ANOVA test followed by Dunnett's post-hoc test). (**B**) Western blot analysis of Agrin, Wnt3a, and Wnt11 in differentiating NSC-34 cells. In each lane 30 µg of total proteins were loaded and actin expression was used as loading control. (**C**) lEVs and sEVs were isolated from NSC-34 during differentiation as indicated in Fig. 1. Whole cell extracts of undifferentiated NSC-34 cells (CB Diff-T0) and extracellular vesicles (lEVs and sEVs) at indicated times were probed with Tsg101, CD81 and CD9, used as EV markers, and Calnexin as the negative control. The figure clearly shows that Wnt11 is present in both lEVs and sEVs whereas Wnt3a is expressed only in sEVs, with a decreasing trend during neurite process development. Five µg of total proteins were loaded in each lane. Molecular weight markers (kDa) are indicated. Original, uncropped immunoblots are reported in Additional File 8 - Fig. S2

the crosstalk between motor neurons and surrounding cells.

NSC-34-derived EVs carry Wnts

Wnts act as morphogens to regulate crucial events of cell fate and development; in the formation of neuronal circuits, Wnts regulate axon guidance, dendritic development, synaptogenesis and synaptic function [43]. More recently, exosomes have emerged as potential carriers for Wnt secretion [14–17, 44]. Interestingly, NGS analysis of the NSC-34 EV-miRNAs highlighted the loading into EVs of many miRNAs involved in the modulation of axon guidance and Wnt signalling pathway (Fig. 3A and B). Since several studies pointed out the role of the Wnt-associated signalling network in NMJ formation, further experiments were performed to investigate whether NSC-34-derived EVs are loaded with Wnts beyond the miRNAs involved in Wnt signalling modulation.

At first, the mRNA expression levels of several Wnts during NSC-34 differentiation was examined (Fig. 4A). Of note, *Wnt1*, *Wnt3*, and *Wnt11* were expressed at levels significantly higher than the other tested Wnts, followed by *Wnt5a* and *Wnt9a*; on the contrary, the expression of other isoforms, such as *Wnt3a*, *Wnt4*, *Wnt7b*, and *Wnt10*, was barely detectable. Interestingly, among the most abundant transcripts *Wnt1* and *Wnt3* increase their expression during NSC-34 differentiation; *Wnt5a* is the only isoform down-regulated, while *Wnt11* is constitutively expressed at high levels. Subsequently, western blotting analyses were performed to investigate whether EVs carry Wnt morphogens into the extracellular environment. The activity of Wnts, Agrin and its coreceptors Lrp4 and MuSK is critical for AChR clustering and thus for NMJ formation. Since in our experimental setup, Agrin protein was barely detectable in NSC-34 cells (Fig. 4B), and it was not found at all in EVs (data not shown), we focused on Wnt4 and Wnt11 which can stimulate clustering, independently from Agrin, directly binding MuSK. Wnt4 is barely detectable both at mRNA level (Fig. 4A) in the whole cell and at protein level in EVs (Fig. 4C; the Wnt4 protein was undetectable in the whole cell, data not shown) [45]. Whereas the other Agrin-independent stimulating Wnt, Wnt11 protein is easily detectable in NSC-34 cell bodies as shown in Fig. 4B, and in both lEVs and sEVs (Fig. 4C). Finally, we evaluated Wnt3a protein expression, one of the best characterised Wnts. As shown in Fig. 4B, Wnt3a shows a decreasing trend during neurite development, and in our hand, it is loaded into sEVs but not lEVs mirroring a reduction during NSC-34 differentiation (Fig. 4C). To confirm Wnt loading into EVs further, well-established markers (Tsg101, CD9 and CD81 and the negative control for sEVs, Calnexin; Fig. 4C) were used to characterise lEVs and sEVs. The obtained results suggest that EVs could modulate NMJ development through Wnts.

NSC-34-derived EVs stimulate C2C12 plasma membrane remodelling favouring AChR clustering

An accurate communication process between the motor neuron and the skeletal muscle fibre is required for proper NMJ assembly, growth, and maintenance. Based on the above-reported observations that either miRNAs or Wnt11, both involved in NMJ formation, are loaded into NSC-34-derived EVs, we investigated whether the EVs from NSC-34 cells (donors) can stimulate plasma membrane remodelling in C2C12 myotubes (targets). To address this question, a transwell co-culture system with C2C12 myotubes (bottom) and differentiated NSC-34 (top) was set up (Fig. 5A); after two days of co-culture, the signals released into the environment, including EVs, induced R-Spondin 2 (*Rspo2*) upregulation and Acetylcholine receptor alpha (*AChR alpha*) downregulation in myotubes, while *ß-catenin* and *Vangl2* were unchanged. These data suggest that NSC-34 and C2C12 cross-talk can lead to myotube membrane remodelling, an initial phase of NMJ formation (Fig. 5B).

Subsequently, to gain insights into the role of NSC-34-derived EVs on the modulation of muscle membrane receptors, an event that precedes the juxtaposition of motor neuron termination to the muscle fibre, C2C12 myotubes were treated with EVs purified from five-day differentiated NSC-34 cells (Diff-T5 lEVs and sEVs). Thus, we aimed to evaluate whether NSC-34-derived EVs could modulate the levels of AChR clustering in myotubes.

Immunofluorescence staining with α-Bungarotoxin (Fig. 5C) allowed us to highlight a significant increase in AChR clusters in response to the EV administration. Morphometric analysis of the AChR clusters showed that lEV and sEV treatments increased the number of AChR clusters per µm of fibre and reduced the cluster area

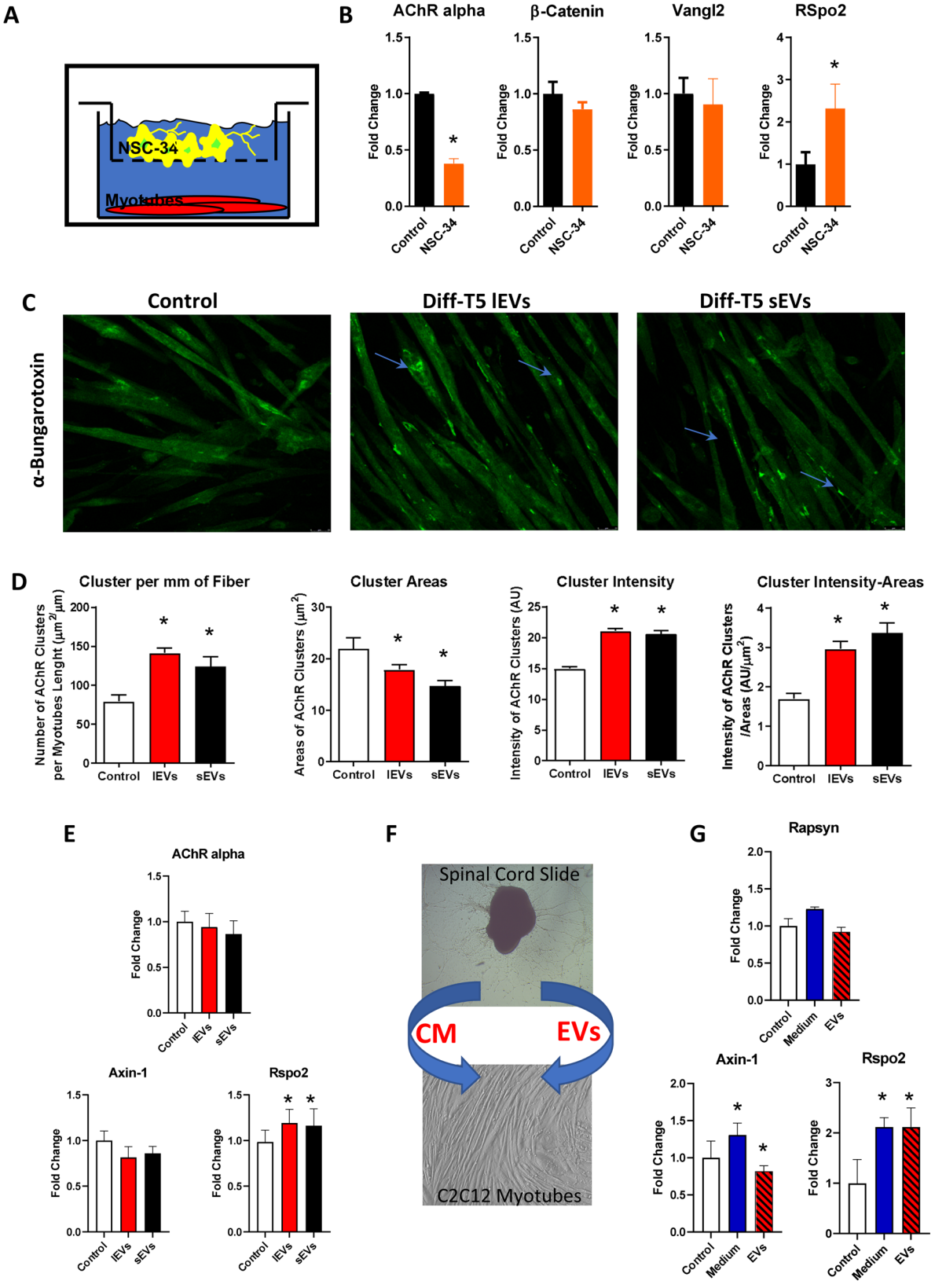

Fig. 5 (See legend on next page.)

(See figure on previous page.)

Fig. 5 Motor neuron-derived EVs stimulate AChR cluster formation in C2C12 plasma membrane. (**A**) C2C12 myotubes and differentiating NSC-34 cells were co-cultured and allowed to interact for 48 h without physical contact thanks to the presence of a membrane filter of 0.4 µm pores interposed between the two cell lines. (**B**) After 48 h co-culture, myotubes were harvested and mRNA extracted to evaluate the gene expression of selected targets; the obtained data show that the presence of NSC-34 cells (and likely their released signals) induced in C2C12 myotubes a decrease and an increase in *AChR alpha* and *Rspo2* mRNAs, respectively ($n = 3$, * $p < 0.05$; t-test). (**C**) The α-Bungarotoxin confocal laser scanning microscopy analysis highlights a significant increase in AChR clusters in response to the EV administration. (**D**) The morphometric analysis of the AChR clusters shows that lEV and sEV treatments increased the number of AChR clusters per µm of fibre and reduces the cluster area; in detail the increase of the fluorescence intensity emitted from clusters in the treated samples, is more evident when the intensity was related to the cluster area (* $p < 0.05$, one-way ANOVA test followed by Dunnett's post-hoc test). (**E**) At the molecular level, lEVs and sEVs induce the stimulation of *Rspo2* in the EV-treated myotubes and a tendency to decrease of *AChR alpha* and *Axin-1* mRNA expression (* $p < 0.05$, one-way ANOVA test followed by Dunnett's post-hoc test). (**F**) An ex vivo model of primary motor neurons derived from spinal cord explants was used to corroborate the results obtained using the NSC-34 model. Total EVs were collected from motor neurons grown for 9–11 days after explantation and used to treat mature myotubes; the conditioned medium (CM) not centrifuged was used to compare bulk with vesicular signals. (**G**) In line with NSC34-derived EV effects, *Rspo2* and *Axin-1* mRNA levels are modulated by motor neuron EVs (* $p < 0.05$, one-way ANOVA test followed by Dunnett's post-hoc test for *Rspo2* and Bonferroni post-hoc test (Medium vs. EVs) for *Axin-1*)

(Fig. 5D). The reduction of cluster area can be explained as a lower diffusion of AChRs on the myotube plasma membrane due to clustering. Finally, the fluorescence intensity emitted from clusters was higher in the treated samples, more clearly when the intensity was related to the cluster area (Fig. 5D). These data are in agreement with the stimulation of *Rspo2* in the EV-treated myotubes, whereas *AChR alpha* and *Axin-1* mRNA expression showed a tendency to decrease (Fig. 5E). *Axin-1* and *Rspo2* modulate Wnt signalling supporting the hypothesis of a possible involvement of the Wnt pathway in stimulating AChR clustering.

According to the results obtained using the NSC-34 in vitro model, we attempted to corroborate our findings using an ex vivo model of primary motor neurons derived from spinal cord explants (Fig. 5F). The EVs were collected from motor neurons grown for 9–11 days after explantation. In detail, conditioned media were collected and ultracentrifuged following a similar protocol used to isolate NSC-34-derived EVs. Still, we no longer separated EVs in different sub-populations due to the low amount of collected EVs and since NSC-34-derived lEVs and sEVs induced overlapping effects on myotubes.

Then, mature myotubes were treated both with the EVs isolated from the ex vivo model of primary motor neurons and motor neuron conditioned medium not centrifuged (CM, soluble and vesicular signals) (Fig. 5F). As shown in Fig. 5G, in line with NSC-34-derived EVs effects, *Rspo2* mRNA levels were higher in C2C12 treated with conditioned medium and EVs than in control samples, while *Axin-1* expression seems to be slightly downregulated in response to EV treatment; conversely, it increased following the treatment with not centrifuged medium. Moreover, *Rapsyn* expression was not modulated in response to both EV treatment and to not centrifuged medium (Fig. 5G).

Altogether, the collected data demonstrate that motoneurons release EVs containing molecular signals, proteins and microRNAs able to stimulate AChR aggregation on the myotube membrane, a preparatory stage of the NMJ formation.

NSC-34-derived EVs act as platforms of integrated molecular signals triggering β-catenin dependent and independent Wnt pathways for AChR clustering

The above reported NGS data showed that EVs secreted from NSC-34 cells are enriched in miRNAs synergically targeting the effectors of the β-catenin dependent Wnt pathway (such as Axin-1, GSK3*β*, CSNK2a2/1a1, APC and, Ppp2R5c) and leading to its activation (Fig. 6A). Furthermore, we demonstrated that NSC-34-derived sEVs shuttle high levels of Wnt11, a Wnt isoform known to stimulate both the canonical and non-canonical Wnt pathways, and low quantities of Wnt3a, a negative modulator of the Wnt signalling [10, 18, 19]. This evidence prompted us to investigate whether sEV administration to C2C12 cells could activate Wnt signalling contributing to AChR clustering.

Since Wnt11 can stimulate AChR clustering even in the absence of Agrin, we first administered Agrin or Diff-T5 NSC-34-derived sEVs to C2C12 myotubes, then AChR clustering was studied. Immunofluorescence staining with α-Bungarotoxin showed AChR cluster formation in the presence of both Agrin and sEVs (Fig. 6B), suggesting that Wnt11 carried by sEVs could directly activate the MuSK receptor and stimulate down-stream signalling leading to AChR clustering.

Moreover, the gene expression analysis by qRT-PCR (Fig. 6C) highlighted *Axin-1* and *β-catenin* mRNA downregulation. Axin-1 is a component of the destruction complex of β-catenin together with adenomatous polyposis coli (APC), glycogen synthase kinase 3 beta (GSK3*β*) and casein kinase (CSNK), indeed *Axin-1* mRNA degradation is compatible with β-catenin-dependent Wnt activation and miR-124-3p activity. Of note, *Rspo2* increased after sEV treatment further corroborating Wnt-dependent AChR clustering (Fig. 6C) [46]. The immunofluorescence analysis evidenced a clear translocation of β-catenin into the nucleus of myotubes treated with NSC-34-derived sEVs (Fig. 6D) Moreover, western blotting analysis of β-catenin active form further supported the sEV positive stimulation of the canonical Wnt signalling (Fig. 6E). This evidence is in agreement with

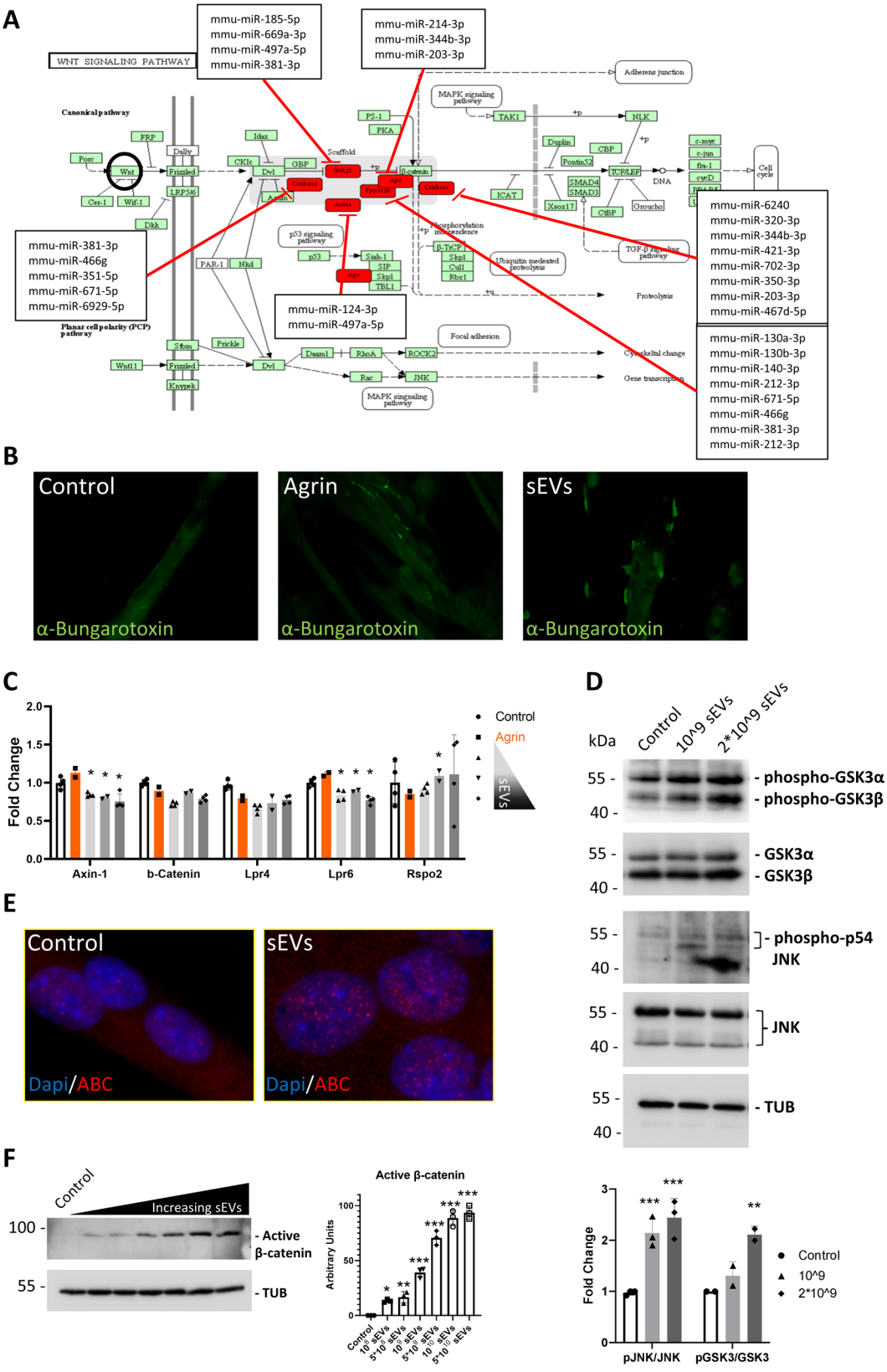

Fig. 6 (See legend on next page.)

(See figure on previous page.)

Fig. 6 NSC-34-derived EVs trigger β-catenin dependent and independent Wnt pathways for AChR clustering. (**A**) Target prediction of NSC-34-derived EV miRNAs and DIANAmirPath analysis of Wnt signalling (Kegg pathway), based on DIANA miRPath v.3.0 program. The miRNAs selected from the first two quartiles of Diff-T 2-T5 lEVs and sEVs have been used for the analysis. The miRNAs highlighted in red target the genes involved in the destruction complex of the *β*-catenin. (**B**) The α-Bungarotoxin confocal laser scanning microscopy analysis highlights a significant increase in AChR clusters in response to the Agrin and sEV treatments. (**C**) Expression analysis of some targets of the Wnt signalling pathway by qPCR analyses in C2C12 myotubes treated with Agrin or increasing quantities of NSC-34 sEVs (sEV concentrations were 5×10^8, 1×10^9, and 5×10^9 particles/mL indicated by symbols). * $p<0.05$, one-way ANOVA test followed by Dunnett's post-hoc test. (**D**) Western blotting analysis: the increased expression of GSK3 inactive form and JNK active form was measured as ratio of the phosphorylated isoform/not phosphorylated isoform. The fold change refers to the control condition (non-treated C2C12 myotubes). ** $p<0.01$, *** $p<0.001$, one-way ANOVA test followed by Dunnett's post-hoc test. (**E**) Immunofluorescence staining of C2C12 myotubes treated with NSC-34-derived sEVs, representative pictures showing the increased nuclear localization of *β*-catenin (red) and DAPI (blue) following EV treatment. (**F**) Western blotting analysis of the *β*-catenin active form in C2C12 myotubes treated with NSC-34 sEVs ranging from 10^8 to 5×10^{10} particles/mL. Tubulin expression was used as loading control. Arbitrary units refer to the control condition. * $p<0.05$; ** $p<0.01$ *** $p<0.001$, one-way ANOVA test followed by Dunnett's post-hoc test. Original, uncropped immunoblots are reported in Additional File 9 - Fig. S3

the accumulation of p-GSK3*β* following treatments with increasing concentration of the NSC-34-derived sEVs (Fig. 6F).

Since Wnt11 could also activate non-canonical Wnt/PCP pathway through the hetero-dimer Lrp4/MuSK, the mRNA expression of *Lrp4* and *Lrp5/6* was also investigated; qRT-PCR data showed *Lrp6* down-regulation, while *Lrp4* mRNA was unchanged suggesting that the formation of the hetero-dimer receptor Lrp4/MuSK could be favoured in response to EV treatment (Fig. 6C). Western blot analysis of JNK, one of the down-stream effectors of MuSK, revealed an increase in p-JNK in response to NSC-34-derived sEVs (Fig. 6F).

The results obtained support the current literature describing the involvement of both canonical and non-canonical signalling pathways in NMJ formation; in fact, the data reported here show that EV treatment induces AChR clustering and this phenomenon is associated with β-catenin translocation into the nucleus, suggesting activation of canonical Wnt signalling. Furthermore, as suggested by the increase in p-JNK following EV treatment, it appears that NSC-34-derived EVs could also activate non-canonical signalling pathways thanks to their complex cargo. Interestingly, EV miRNAs appear to down-regulate *Lrp6* mRNA, consequently *Lrp6* mRNA decrease could favour the formation of the Lrp4/Musk receptor dimer, further supporting the idea of the activation of Wnt11-Lrp4/Musk-JNK axis.

EVs carrying Wnt11 induce GSK3β phosphorylation

Previous experiments suggested that motor neuron-derived EVs may contribute to the early stages of NMJ development by inducing the clustering of AChRs through the activation of canonical and non-canonical Wnt signalling pathways. In this scenario, we hypothesised that Wnt11 could act as an upstream stimulus, while the miRNAs enriched in NSC-34 EVs could fine-tune the downstream effectors of Wnt11. In an attempt to dissect the role of Wnt11 and miRNAs in this process, we forced the expression of exogenous Wnt11-HA tag fusion protein in Hek293 cells, then we collected sEVs from transformed Hek293 and used them to treat myotubes. After 18 h treatment, the modulation of Wnt signalling was investigated. First, we performed NTA of sEVs isolated by serial ultracentrifugation (Fig. 7A), then using western blot analysis we showed that the Hek293 cells over-expressing Wnt11-HA tag fusion protein secreted sEVs positive for CD63, a typical exosomal marker, and Wnt11 (Fig. 7B). Although, sEVs from wild-type Hek293 show the expression of low levels of endogenous Wnt11, the positivity for HA tag only in transformed Hek293 cells unambiguously demonstrates the loading of exogenous Wnt11-HA tag into sEVs (Fig. 7B). Notably, this evidence extends the finding that EVs carry Wnt11. Subsequently, EVs loaded with exogenous Wnt11 but not motor neuron-derived miRNAs were administered to myotubes, and the WNT pathway was studied. Figures 7C and D clearly show that the administration of Hek-Wnt11 sEVs to myotubes induced GSK3β phosphorylation; interestingly a slight increase in GSK3β phosphorylation was also observed for wt Hek sEVs (Fig. 7C and D), probably due to the presence of low levels of endogenous Wnt11. Evaluation of downstream markers of canonical Wnt signalling revealed that, although Wnt11 led to the GSK3β phosphorylation, the corresponding activation of β-catenin was not detected (Fig. 7C). These findings suggest that, in our experimental setup, NSC-34-derived miRNAs seem to be crucial for an efficient β-catenin activation. Moreover, Hek-Wnt11 sEV administration to myotubes did not induce a significant JNK phosphorylation (Fig. 7C and D). Overall, these data suggest that, without NSC-34 miRNAs, Wnt11 has a negligible effect on activating the non-canonical Wnt signalling pathway. However, it appears to activate GSK3β phosphorylation, a typical step in the canonical pathway.

Discussion

Recent findings from the *Drosophila* larval NMJ illustrate how intra- and inter-cellular membrane trafficking and signalling pathways, particularly Wingless, bone morphogenic protein and c-Jun-activated kinase pathways, impinge on the establishment and stability of NMJ arbours [47].

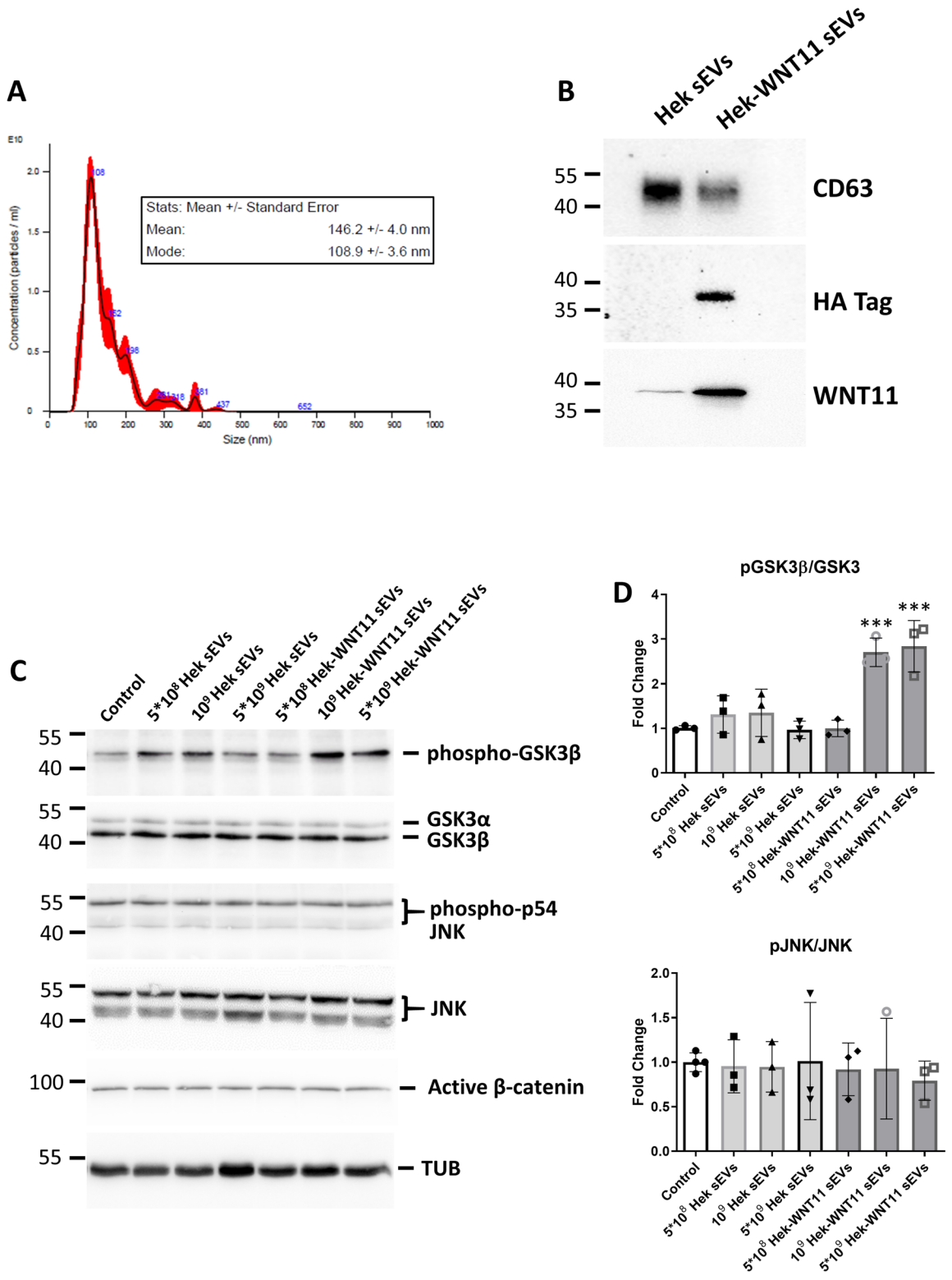

Fig. 7 (See legend on next page.)

(See figure on previous page.)

Fig. 7 Hek-WNT11 sEVs induce GSK3β phosphorylation. (**A**) NTA distribution plot of the hydrodynamic diameter size of Hek-WNT11 sEVs. (**B**) The Western blot analysis of the sEVs secreted by wild type and WNT11-HA tag-overexpressing HEK cells shows the presence of the well-established exosomal marker CD63, and the WNT11 or HA tag (10 µg of total proteins were loaded per lane). Molecular weight markers (kDa) are indicated. (**C**) Western blot analysis of GSK3α/β, JNK and β-catenin in C2C12 myotubes treated with increasing concentrations of Hek sEVs (lanes 2–4) or Hek-WNT11 sEVs (lanes 5–7) as indicated in the figure. Non-treated C2C12 myotubes represent the control (lane 1); Tubulin was used as the housekeeping protein. Molecular weight markers (kDa) are indicated. Original, uncropped immunoblots are reported in Additional File 11 - Fig. S4. (**D**) Expression of GSK3 inactive form e JNK active form was measured as ratio of the phosphorylated isoform/not phosphorylated isoform. The fold change refers to the control condition. *** $p < 0.001$, one-way ANOVA test followed by Dunnett's post-hoc test

In this study, we provide evidence that the EVs released by motor neurons are loaded with miRNAs and Wnts which are involved in modulating the remodelling of the postsynaptic muscle membrane. Indeed, we found that NSC-34-derived EVs induce AChR clustering in myotubes plasma membrane, a well-known process that occurs during the early stages of NMJ development. This process is considered essential for the juxtaposition of motor neuron terminals.

A growing body of evidence shows that miRNAs play a significant role in motor neuron development, especially at the NMJ. For example, the lack of expression of miR-124, miR-125 and let-7 in *Drosophila* is associated with defects in NMJ function [48, 49] and phenotype [48, 50]. Moreover, miR-218 is crucial for establishing motor neuron identity regulating neuromuscular synapses, membrane excitability and motoneuron survival [51]. Other miRNAs, such as miR-310/313, as well as miR-153, are involved in the regulation of synaptic homeostasis [52]. MiRNAs are distributed in neuronal compartments where they can regulate mRNA translation, however accumulating evidence demonstrates that miRNAs are also secreted enwrapped into EVs contributing to information exchange within the nervous system [53].

The herein-reported data open a new exciting scenario for the involvement of EV-derived miRNAs in NMJ establishment and function. In this study, we observed an upregulation of miR-9 and miR-124 in NSCs during neuronal differentiation, confirming previous evidence that these two miRNAs exert synergistic effects on neuronal differentiation and dendritic tree complexity [54]. We focused on the analysis of the miRNAs loaded into NSC-34-derived EVs and we found that EVs carry a dynamic network of miRNAs, including MotoMiRs (i.e. miR-9, miR-124, miR-218), which are critical for the development, viability and regeneration of motoneurons [55]. Although the effect of a single microRNA on the expression levels of a specific transcript may appear small, the combinatory effects of different microRNAs on a same target, or on several targets within the same signalling pathway, could become noteworthy [55, 56]. Indeed, NGS analysis highlighted that EVs secreted from well-formed motor neurons contain a pool of miRNAs specifically enriched during motoneuron differentiation, which targets the transducers of the Wnt signalling, thus suggesting that these miRNAs can modulate Wnt signalling activation in the recipient cells.

Starting from the evidence here reported, that EVs are enriched in miRNAs involved in Wnt signalling and axon guidance, and contain the morphogens Wnts, fundamental in NMJ formation, we demonstrated that NSC-34-derived EVs induce the formation of AChR clusters, an essential step preceding NMJ formation. Using in vitro and ex-vivo experimental models, we also found that AChR clustering was paralleled with gene expression modulation; in more detail we highlighted *AChR alpha*, *Axin-1* and *Lrp6* mRNA expression decrease, whereas *Rspo2* increases in response to EV treatments. *AChR alpha* mRNA downregulation could appear to be contradictory to AChR cluster formation, but it actually corroborates previous data from Liao et al. [57]. Liao's group demonstrated that muscle-specific overexpression of AChR alpha (CHRNA1) not only causes muscle fibre atrophy, but also results in the loss of presynaptic motor nerve endings and a decrease in compound muscle action potentials. These findings suggest that CHRNA1 overexpression in muscle may activate retrograde signalling causing the degeneration of presynaptic motor nerve endings and increasing muscle fibre denervation.

In line with this predicted data, we highlighted *Axin-1* and *Lrp-6* mRNA decrease, two targets of the identified MotoMiRs, and an increase in GSK3β phosphorylation (p-GSK3β, inactive isoform), a well-known key transducer of the β-catenin-dependent Wnt signalling, in myotubes incubated with NSC-34-derived EVs. In colorectal cancer, Axin-2 repression helps in prolonging the duration of Wnt signalling by blocking the negative feedback loop as well as increasing the duration of Wnt target genes expression [58]. Because Axin is present in cells at the rate-limiting level, a reduction in Axin levels would lead to β-catenin stabilisation [59]. Furthermore, among the miRNAs enriched in NSC-34-derived EVs, it has been previously shown that miR-9 and miR-124 together target and strongly suppress the small GTP-binding protein Rap2a, which is in turn a suppressor of GSK3β leading to a decrease in its phosphorylation (Ser-9 phosphorylation). In this way, the synergistic action of miR-9 and miR-124 could lead to promotion of GSK3β inhibition and, as a result, boost neuronal maturation and dendritic branching [54]. This evidence agrees with our current data showing that NSC-34-derived EVs

are enriched in miR-9 and miR-124, and the EV treatment of myotubes increases GSK3β phosphorylation and β-catenin translocation to the nucleus.

Furthermore, since Wnt morphogens are hydrophobic molecules, owing to lipid post-translational modifications, we asked whether they can be trafficked into extracellular space through EVs. It has been widely demonstrated that Wnts act as autocrine as well as paracrine signalling molecules between Wnt-producing and Wnt-receiving cells, however how they are transported to fulfil their paracrine signalling functions is still unclear. Several mechanisms have been proposed to mediate intercellular Wnt transport, including Wnt-binding proteins, cytonemes, lipoproteins, and exosomes [60].

A role for exosomes in transporting Wnt proteins was first reported in the *Drosophila* NMJ [15]. Pioneering studies by Budnik [20, 61] suggested that Wg is transferred in exosomes through binding to the exosomal protein, Evi, which is released from presynaptic terminals [16]. In this model, Wg is carried across the synaptic cleft by Wls -containing exosomes to influence synaptic growth, function and plasticity. This observation is supported by a study that showed Wnt3a can localise with exosomes from Hek293 cells [16]. By using TSG101 protein as an exosomal marker, lysate immunoblot analysis of Wnt-expressing cells revealed the presence of Wnt3a and Wnt5a in the exosomal fractions. Furthermore, in vivo staining of the *Drosophila* wing disc revealed colocalization of Wg and the exosomal marker CD63-GFP in both intracellular MVBs and the extracellular space, although this was only a fraction of the total Wg staining [16]. Moreover, studies at the zebrafish NMJ have demonstrated that Wnt11r binds to MuSK and is required for the formation of aneural AChR clusters [62].

In CNS injury, fibroblast-derived exosomes promote axonal regeneration by inducing re-localisation of neuronal Wnt10b to lipid rafts, which promotes CNS repair through mTOR pathway activation [44]. All these data are in agreement with our current data showing that Wnt11, Wnt4 and Wnt3a are carried by NSC-34-derived EVs.

Recent evidence suggests that Wnts may regulate vertebrate NMJ formation by directly interacting with Lrp4 and MuSK. Besides MuSK, several Wnts including Wnt7a, Wnt9a, and Wnt11 could also directly interact with Lrp4. Of these, treatment with soluble Wnt11 increases the number of AChR clusters in myotubes, in the absence of exogenous Agrin [10].

Since Agrin was barely detectable in NSC-34 cells and absent in EVs, we focused on Wnt11 because, first, it is expressed at high levels in differentiated NSC-34 cells, and second, Wnt11 stimulates AChR clustering in an Agrin-independent manner. Our data demonstrate that Wnt11 is loaded into EVs and sEVs stimulate aneural AChR clustering through a process associated with canonical and non-canonical Wnt pathway stimulation, as highlighted by β-catenin stabilisation and nuclear translocation, as well as JNK activation and *Rspo2* mRNA upregulation. Of note, the down-regulation of the *Lrp6* mRNA, probability due to EV-miRNA action, could alter the balance between Lrp6 and Lrp4 favouring MuSK/Lrp4 hetero-dimer formation and ultimately Wnt11 stimulation. The key role of MotoMiRs in modulating Wnt signalling is further supported by the results obtained using HEK-Wnt11-derived EVs, which are enriched in Wnt11, but not in NSC-34-derived microRNAs. Our data show that HEK-Wnt11 sEVs only partially activate the canonical Wnt pathway when administered to myotubes, confirming the importance of the synergistic action of microRNAs and morphogens (e.g. Wnt11) carried by NSC-34-derived EVs.

Conclusions

On the whole, it has been extensively demonstrated that extracellular vesicles are naturally occurring biological platforms able to carry multimodal signals, such as lipids, proteins, nucleic acids (mRNA, miRNAs, lncRNAs, and DNA), and small soluble molecules from a source cell to a target cell [63]. Interestingly, here we reported that neuron-derived EVs can deliver to a target muscle cell integrated signal units consisting of (i) the signal, i.e. Wnts, necessary for the activation of the Wnt signalling pathway, and (ii) some key miRNAs, i.e. MotoMiRs, able to finely tune the effectors (transducers) of the Wnt signalling pathway, such as GSK3β, JNK and β-catenin, thereby potentiating their action. As outlined, this data shed light on the complex mechanisms underpinning NMJ establishment, where, in addition to soluble factors, EVs can mediate the motor neuron/muscle crosstalk, inducing AChR clustering. Further studies will be needed to identify which miRNAs are essential in the stimulation of AChR clustering.

Furthermore, current and future results will also provide insights into whether EVs can be applied in the treatment of motor neuron lesions.

Abbreviations

AChR	Acetylcholine receptor
Ctnnb1	β-catenin
EV	Extracellular vesicle
Fzd	Frizzled receptors
Lrp	Low density lipoprotein receptor-related protein
MuSK	Muscle-specific tyrosine kinase
NMJ	Neuromuscular junction
Wg	Wingless
Wnt	Wingless/Integrated

Supplementary Information

The online version contains supplementary material available at https://doi.org/10.1186/s12964-025-02312-x.

Additional File 1: Small RNA sequence analysis. Raw data were generated from the Illumina NextSeq 500 system. Raw counts were normalised using DESeq2 bioconductor package (http://bioconductor.org/). Data were analysed using Genespring GX software v. 14.8 (Agilent Technologies). miRNAs expressed in at least one sample are reported (n = 353).

Additional file 2: List of primers utilized for quantitative Real Time PCR.

Additional file 3: Table of the primary and secondary antibodies used for western blot analyses. Dilutions used in the experiments and company information are reported.

Additional file 4: Venn diagram of the total miRNAs identified in sEVs and lEVs released from NSC-34 (Diff-T2 and Diff-T5). The miRNAs detected in at least two independent reads were considered for the analysis.

Additional file 5: Venn diagram of the miRNAs identified in NSC-34-derived sEVs at Diff-T2 and Diff-T5. The miRNAs detected in at least two independent reads were considered for the analysis; significantly down- and up-regulated miRNAs were reported in red and green, respectively.

Additional file 6: Venn diagram of the miRNAs identified in NSC-34-derived lEVs at Diff-T2 and Diff-T5. The miRNAs detected in at least two independent reads were considered for the analysis; significantly down- and up-regulated miRNAs were reported in red and green, respectively.

Additional file 7: Fig. S1. Original, uncropped immunoblots of Fig. 1G.

Additional file 8: Fig. S2. Original, uncropped immunoblots of Fig. 4B C.

Additional file 9: Fig. S3. Original, uncropped immunoblots of Fig. 6D F.

Additional file 10: cell viability of NSC-34 during the motor neuron differentiation process.

Additional file 11: Fig. S4. Original, uncropped immunoblots of Fig. 7B C.

Acknowledgements
We thank Alessandro Fanzani and Andrea Frontini and for many stimulating discussions. We are grateful to our laboratory members for their continuous support. We apologize to all colleagues whose work could not be cited as a result of space limitations.

Author contributions
M.G., R.A., E.P. and P.C. designed the experiments. R.A., E.P., P.C., S.M., I.P., A.C., M.B., and G.M. performed the experiments. M.G., R.A., E.P., P.C., M.S., M.F., F.O. and V.S. analyzed the data. M.G., R.A., E.P. and P.C. wrote the original draft, and all Authors commented on previous versions of the manuscript. M.G., F.C. and E.F. revised the manuscript. All Authors read and approved the final manuscript.

Funding
This work was supported by the Italian Ministry of Health (under Grant Ricerca Finalizzata n. GR-2011-02350264).

Data availability
The manuscript has data included has supplementary materials. Furthermore, original data are available from the corresponding author on reasonable request.

Declarations

Ethical approval and consent to participate
All animal care and handling procedures were approved by the Institutional Animal Care and Use Committee of Istituto Italiano di Tecnologia, Genova, Italy.

Consent for publication
All authors read and approved the final manuscript.

Competing interests
The authors declare no competing interests.

Author details
[1]Department of Biomolecular Sciences, University of Urbino Carlo Bo, Via I Maggetti, 26, Urbino 61029, Italy
[2]Department of Medical and Surgical Sciences (DIMEC), University of Bologna, Bologna, Italy
[3]IRCCS Azienda Ospedaliero-Universitaria of Bologna, Bologna, Italy
[4]IRCCS INRCA, Ancona, Italy
[5]Department of Clinical and Molecular Sciences (DISCLIMO), Polytechnic University of Marche, Ancona, Italy
[6]Department of Life Sciences, University of Trieste, Trieste, Italy
[7]Center for Synaptic Neuroscience and Technology, Istituto Italiano di Tecnologia, Genova 16132, Italy
[8]Department of Human Sciences for the Promotion of Quality of Life, University San Raffaele, Roma, Italy

Received: 8 August 2024 / Accepted: 14 June 2025
Published online: 01 August 2025

References

1. Slater C. The structure of human neuromuscular junctions: some unanswered molecular questions. Int J Mol Sci. 2017;18:2183. https://doi.org/10.3390/ijms18102183.
2. Li L, Xiong W-C, Mei L. Neuromuscular junction formation, aging, and disorders. Annu Rev Physiol. 2018;80:159–88. https://doi.org/10.1146/annurev-physiol-022516-034255.
3. Kummer TT, Misgeld T, Sanes JR. Assembly of the postsynaptic membrane at the neuromuscular junction: paradigm lost. Curr Opin Neurobiol. 2006;16:74–82. https://doi.org/10.1016/j.conb.2005.12.003.
4. Anderson MJ, Cohen MW. Nerve-induced and spontaneous redistribution of acetylcholine receptors on cultured muscle cells. J Physiol. 1977;268:757–73. https://doi.org/10.1113/jphysiol.1977.sp011880.
5. Zong Y, Zhang B, Gu S, et al. Structural basis of agrin–LRP4–MuSK signaling. Genes Dev. 2012;26:247–58. https://doi.org/10.1101/gad.180885.111.
6. Tintignac LA, Brenner H-R, Rüegg MA. Mechanisms regulating neuromuscular junction development and function and causes of muscle wasting. Physiol Rev. 2015;95:809–52. https://doi.org/10.1152/physrev.00033.2014.
7. Gordon LR, Gribble KD, Syrett CM, Granato M. Initiation of synapse formation by Wnt-induced musk endocytosis. Development. 2012;139:1023–33. https://doi.org/10.1242/dev.071555.
8. Nusse R. Wnt signaling. Cold Spring Harb Perspect Biol. 2012;4:a011163–011163. https://doi.org/10.1101/cshperspect.a011163.
9. Avilés EC, Pinto C, Hanna P, et al. Frizzled-9 impairs acetylcholine receptor clustering in skeletal muscle cells. Front Cell Neurosci. 2014;8. https://doi.org/10.3389/fncel.2014.00110.
10. Zhang B, Liang C, Bates R, et al. Wnt proteins regulate acetylcholine receptor clustering in muscle cells. Mol Brain. 2012;5:7. https://doi.org/10.1186/1756-6606-5-7.
11. Messéant J, Dobbertin A, Girard E, et al. MuSK Frizzled-Like domain is critical for mammalian neuromuscular junction formation and maintenance. J Neurosci. 2015;35:4926–41. https://doi.org/10.1523/JNEUROSCI.3381-14.2015.
12. Barik A, Zhang B, Sohal GS, et al. Crosstalk between Agrin and wnt/signaling pathways in development of vertebrate neuromuscular junction. Dev Neurobiol. 2014;74:828–38. https://doi.org/10.1002/dneu.22190.
13. Kim N, Stiegler AL, Cameron TO, et al. Lrp4 is a receptor for Agrin and forms a complex with musk. Cell. 2008;135:334–42. https://doi.org/10.1016/j.cell.2008.10.002.
14. Luga V, Zhang L, Viloria-Petit AM, et al. Exosomes mediate stromal mobilization of autocrine Wnt-PCP signaling in breast Cancer cell migration. Cell. 2012;151:1542–56. https://doi.org/10.1016/j.cell.2012.11.024.
15. Korkut C, Ataman B, Ramachandran P, et al. Trans-Synaptic transmission of vesicular Wnt signals through evi/wntless. Cell. 2009;139:393–404. https://doi.org/10.1016/j.cell.2009.07.051.
16. Gross JC, Chaudhary V, Bartscherer K, Boutros M. Active Wnt proteins are secreted on exosomes. Nat Cell Biol. 2012;14:1036–45. https://doi.org/10.1038/ncb2574
17. Beckett K, Monier S, Palmer L, et al. Drosophila S2 cells secrete wingless on Exosome-Like vesicles but the wingless gradient forms independently of exosomes. Traffic. 2013;14:82–96. https://doi.org/10.1111/tra.12016.
18. Koles K, Budnik V. Exosomes go with the Wnt. Cell Logist. 2012;2:169–73. https://doi.org/10.4161/cl.21981.

19. Koles K, Budnik V. Wnt signaling in neuromuscular junction development. Cold Spring Harb Perspect Biol. 2012;4. https://doi.org/10.1101/cshperspect.a008045.
20. Korkut C, Li Y, Koles K, et al. Regulation of postsynaptic retrograde signaling by presynaptic exosome release. Neuron. 2013;77:1039–46. https://doi.org/10.1016/j.neuron.2013.01.013.
21. Théry C, Ostrowski M, Segura E. Membrane vesicles as conveyors of immune responses. Nat Rev Immunol. 2009;9:581–93. https://doi.org/10.1038/nri2567.
22. Simons M, Raposo G. Exosomes – vesicular carriers for intercellular communication. Curr Opin Cell Biol. 2009;21:575–81. https://doi.org/10.1016/j.ceb.2009.03.007.
23. Hessvik NP, Llorente A. Current knowledge on exosome biogenesis and release. Cell Mol Life Sci. 2018;75:193–208. https://doi.org/10.1007/s00018-017-2595-9.
24. Sharma P, Schiapparelli L, Cline HT. Exosomes function in cell–cell communication during brain circuit development. Curr Opin Neurobiol. 2013;23:997–1004. https://doi.org/10.1016/j.conb.2013.08.005
25. Zhang G, Yang P. A novel cell-cell communication mechanism in the nervous system: exosomes. J Neurosci Res. 2018;96:45–52. https://doi.org/10.1002/jnr.24113.
26. Onyido EK, Sweeney E, Nateri AS. Wnt-signalling pathways and MicroRNAs network in carcinogenesis: experimental and bioinformatics approaches. Mol Cancer. 2016;15:56. https://doi.org/10.1186/s12943-016-0541-3
27. Haramati S, Chapnik E, Sztainberg Y et al. (2010) miRNA malfunction causes spinal motor neuron disease. Proceedings of the National Academy of Sciences 107:13111–13116. https://doi.org/10.1073/pnas.1006151107
28. Nesler KR, Sand RI, Symmes BA, et al. The MiRNA pathway controls rapid changes in Activity-Dependent synaptic structure at the Drosophila melanogaster neuromuscular junction. PLoS ONE. 2013;8:e68385. https://doi.org/10.1371/journal.pone.0068385.
29. Kaufmann N, DeProto J, Ranjan R, et al. Drosophila Liprin-α and the receptor phosphatase Dlar control synapse morphogenesis. Neuron. 2002;34:27–38. https://doi.org/10.1016/S0896-6273(02)00643-8.
30. Ferri P, Barbieri E, Burattini S, et al. Expression and subcellular localization of myogenic regulatory factors during the differentiation of skeletal muscle C2C12 myoblasts. J Cell Biochem. 2009;108:1302–17. https://doi.org/10.1002/jcb.22360.
31. Welsh JA, Goberdhan DCI, O'Driscoll L, et al. Minimal information for studies of extracellular vesicles (MISEV2023): from basic to advanced approaches. J Extracell Vesicles. 2024;13. https://doi.org/10.1002/jev2.12404.
32. Dobin A, Davis CA, Schlesinger F, et al. STAR: ultrafast universal RNA-seq aligner. Bioinformatics. 2013;29:15–21. https://doi.org/10.1093/bioinformatics/bts635.
33. Guescini M, Sisti D, Rocchi MBL, et al. A new real-time PCR method to overcome significant quantitative inaccuracy due to slight amplification Inhibition. BMC Bioinformatics. 2008;9. https://doi.org/10.1186/1471-2105-9-326.
34. Pfaffl MW. A new mathematical model for relative quantification in real-time RT-PCR. Nucleic Acids Res. 2001;29:e45–445. https://doi.org/10.1093/nar/29.9.e45.
35. Cashman NR, Durham HD, Blusztajn JK, et al. Neuroblastoma × spinal cord (NSC) hybrid cell lines resemble developing motor neurons. Dev Dyn. 1992;194:209–21. https://doi.org/10.1002/aja.1001940306.
36. Lu Y-L, Yoo AS. (2018) Mechanistic insights into MicroRNA-Induced neuronal reprogramming of human adult fibroblasts. Front Neurosci 12:. https://doi.org/10.3389/fnins.2018.00522
37. Zhao C, Sun G, Li S, Shi Y. A feedback regulatory loop involving microRNA-9 and nuclear receptor TLX in neural stem cell fate determination. Nat Struct Mol Biol. 2009;16:365–71. https://doi.org/10.1038/nsmb.1576.
38. Marassi V, Maggio S, Battistelli M, et al. An ultracentrifugation – hollow-fiber flow field-flow fractionation orthogonal approach for the purification and mapping of extracellular vesicle subtypes. J Chromatogr A. 2021;1638:461861. https://doi.org/10.1016/j.chroma.2020.461861.
39. Varcianna A, Myszczynska MA, Castelli LM et al. (2019) Micro-RNAs secreted through astrocyte-derived extracellular vesicles cause neuronal network degeneration in C9orf72 ebiomedicine 40:626–35. https://doi.org/10.1016/j.ebiom.2018.11.067
40. Vlachos IS, Zagganas K, Paraskevopoulou MD, et al. DIANA-miRPath v3.0: Deciphering MicroRNA function with experimental support. Nucleic Acids Res. 2015;43:W460–6. https://doi.org/10.1093/nar/gkv403.
41. Lu T-P, Lee C-Y, Tsai M-H, et al. MiRSystem: an integrated system for characterizing enriched functions and pathways of MicroRNA targets. PLoS ONE. 2012;7:e42390. https://doi.org/10.1371/journal.pone.0042390.
42. Wu H, Xiong WC, Mei L. To build a synapse: signaling pathways in neuromuscular junction assembly. Development. 2010;137:1017–33. https://doi.org/10.1242/dev.038711.
43. Park M, Shen K. WNTs in synapse formation and neuronal circuitry. EMBO J. 2012;31:2697–704. https://doi.org/10.1038/emboj.2012.145.
44. Tassew NG, Charish J, Shabanzadeh AP, et al. Exosomes mediate mobilization of autocrine Wnt10b to promote axonal regeneration in the injured CNS. Cell Rep. 2017;20:99–111. https://doi.org/10.1016/j.celrep.2017.06.009.
45. Ohkawara B, Ito M, Ohno K. Secreted signaling molecules at the neuromuscular junction in physiology and pathology. Int J Mol Sci. 2021;22:2455. https://doi.org/10.3390/ijms22052455.
46. Nakashima H, Ohkawara B, Ishigaki S, et al. R-spondin 2 promotes acetylcholine receptor clustering at the neuromuscular junction via Lgr5. Sci Rep. 2016;6:28512. https://doi.org/10.1038/srep28512.
47. Deshpande M, Rodal AA. The crossroads of synaptic growth signaling, membrane traffic and neurological disease: insights from Drosophila. Traffic. 2016;17:87–101. https://doi.org/10.1111/tra.12345.
48. Sun K, Westholm JO, Tsurudome K, et al. Neurophysiological defects and neuronal gene deregulation in Drosophila mir-124 mutants. PLoS Genet. 2012;8:e1002515. https://doi.org/10.1371/journal.pgen.1002515.
49. Zhu F, Liu J-L, Li J-P, et al. MicroRNA-124 (miR-124) regulates Ku70 expression and is correlated with neuronal death induced by ischemia/reperfusion. J Mol Neurosci. 2014;52:148–55. https://doi.org/10.1007/s12031-013-0155-9.
50. Caygill EE, Johnston LA. Temporal regulation of metamorphic processes in Drosophila by the let-7 and miR-125 heterochronic MicroRNAs. Curr Biol. 2008;18:943–50. https://doi.org/10.1016/j.cub.2008.06.020.
51. Amin ND, Bai G, Klug JR et al. (2015) Loss of motoneuron-specific microRNA-218 causes systemic neuromuscular failure. Science (1979) 350:1525–1529. https://doi.org/10.1126/science.aad2509
52. Tsurudome K, Tsang K, Liao EH, et al. The Drosophila miR-310 cluster negatively regulates synaptic strength at the neuromuscular junction. Neuron. 2010;68:879–93. https://doi.org/10.1016/j.neuron.2010.11.016.
53. Janas AM, Sapoń K, Janas T, et al. Exosomes and other extracellular vesicles in neural cells and neurodegenerative diseases. Biochim Et Biophys Acta (BBA) - Biomembr. 2016;1858:1139–51. https://doi.org/10.1016/j.bbamem.2016.02.011.
54. Xue Q, Yu C, Wang Y, et al. miR-9 and miR-124 synergistically affect regulation of dendritic branching via the AKT/GSK3β pathway by targeting Rap2a. Sci Rep. 2016;6:26781. https://doi.org/10.1038/srep26781.
55. Liu N, Olson EN. MicroRNA regulatory networks in cardiovascular development. Dev Cell. 2010;18:510–25. https://doi.org/10.1016/j.devcel.2010.03.010.
56. Small EM, Olson EN. Pervasive roles of MicroRNAs in cardiovascular biology. Nature. 2011;469:336–42. https://doi.org/10.1038/nature09783.
57. Liao Z, Xiao M, Chen J, et al. CHRNA1 induces sarcopenia through neuromuscular synaptic elimination. Exp Gerontol. 2022;166:111891. https://doi.org/10.1016/j.exger.2022.111891
58. Lustig B, Jerchow B, Sachs M, et al. Negative feedback loop of Wnt signaling through upregulation of Conductin/Axin2 in colorectal and liver tumors. Mol Cell Biol. 2002;22:1184–93. https://doi.org/10.1128/MCB.22.4.1184-1193.2002
59. Wu D, Pan W. GSK3: a multifaceted kinase in Wnt signaling. Trends Biochem Sci. 2010;35:161–8. https://doi.org/10.1016/j.tibs.2009.10.002.
60. Routledge D, Scholpp S. Mechanisms of intercellular Wnt transport. Development. 2019;146. https://doi.org/10.1242/dev.176073.
61. Koles K, Nunnari J, Korkut C, et al. Mechanism of evenness interrupted (Evi)-Exosome release at synaptic boutons. J Biol Chem. 2012;287:16820–34. https://doi.org/10.1074/jbc.M112.342667.
62. Jing L, Lefebvre JL, Gordon LR, Granato M. Wnt signals organize synaptic Prepattern and axon guidance through the zebrafish unplugged/musk receptor. Neuron. 2009;61:721–33. https://doi.org/10.1016/j.neuron.2008.12.025.
63. Holm MM, Kaiser J, Schwab ME. Extracellular vesicles: multimodal envoys in neural maintenance and repair. Trends Neurosci. 2018;41:360–72. https://doi.org/10.1016/j.tins.2018.03.006.

Publisher's note